

**Modeling, Detection, And  
Localization of High-Impedance Faults  
In Low-Voltage Distribution Feeders**

Fabian Marcel Uriarte

Thesis submitted to the Faculty of the Virginia Tech Polytechnic Institute  
and State University in partial fulfillment of the requirement for the degree  
of

**MASTER OF SCIENCE**  
**in**  
**Electrical Engineering**

Virgilio Centeno, Chairman

Jaime De La Reelopez

Yilu Liu

December 15, 2003

Blacksburg, Virginia

Keywords: HIF, Power Distribution System, Sectionalizer, Harmonics, Phase Angle

Copyright by Fabian Marcel Uriarte

ALL RIGHTS RESERVED

# **Modeling, Detection, And Localization of High-Impedance Faults In Low-Voltage Distribution Feeders**

Fabian Marcel Uriarte

(ABSTRACT)

High-impedance faults (HIFs) on distribution feeders are abnormal electrical conditions that cannot be detected by conventional protection schemes. These faults pose a threat on human lives when neighboring objects become in contact with the line's bare and energized conductors. An accurate electrical model for a HIF is implemented to investigate typical patterns in the line's current that allow for the detection of these faults. The occurrence of HIFs is detected with harmonic-current phase analysis and localized with recloser-sectionalyzer technology as presented in this work. A sectionalizer algorithm is then presented showing the decision criteria for HIF declaration and shown to discriminate against nominal behavior in distribution feeders of similar harmonic content. Finally, it is shown that the algorithm will not produce a misreading when a current transformer enters saturation.

## ACKNOWLEDGEMENT

The author wishes to express sincere appreciation to Professors Glanville, Shaibani, Cooper, Thweatt and advisors Taylor, Kegley, and Graham for their early faith and assistance during my undergraduate studies.

In addition, special thanks to Juancarlo Depablos whose familiarity with the needs and ideas was helpful during the early simulation phase of this undertaking. Just as well for my undergraduate power systems professors, graduate advisor, and professional friend Virgilio Centeno. Your faith in my capabilities gave me tremendous encouragement throughout graduate studies.

Un agradecimiento grandioso a mis padres que siempre tuvieron fé en que saliera adelante algun día. A mi padre por instruirme en el camino de la educación; a mi madre por siempre estar ahí cuando más la necesité; a mi hermano por apoyarme y enseñarme muy de niño técnicas matemáticas.

# TABLE OF CONTENTS

ACKNOWLEDGEMENT .....	iii
TABLE OF CONTENTS .....	iv
LIST OF FIGURES .....	v
LIST OF TABLES.....	vii
Chapter 1: High-Impedance Faults .....	1
1.1. Introduction.....	1
1.2. Statement of Problem.....	2
1.3. Purpose of Study .....	3
1.4. Other Work in This Area.....	6
Chapter 2: Simulation Software .....	10
2.1. Ansoft Simplorer®.....	10
Chapter 3: Electrical Load Models .....	13
3.1. Distribution Feeder .....	13
3.2. Transmission Cables .....	14
3.3. Induction Motor .....	15
3.4. Industrial Heater .....	21
3.5. Voltage Transformers .....	22
3.6. High-Impedance Fault Model.....	25
3.7. Summary of Modeled Loads .....	30
Chapter 4: Modeling of Saturable Current Transformers (CTs) .....	33
4.1. The Need for Modeling CTs.....	33
4.2. Impact of Saturated CTs in Distribution Feeders .....	34
4.3. Modeling CTs from Hysteresis Loops .....	35
4.4. Comparison between CT and HIF Curves.....	42
Chapter 5: Algorithm Criteria and Discussion .....	43
5.1. Using the Third-Harmonic Current-Angle.....	43
Chapter 6: Simulation Results.....	48
6.1. A Foreword on the Results.....	48
6.2. Fault after First Sectionalizer.....	50
6.3. Fault after Second Sectionalizer.....	52
6.4. Fault after Third Sectionalizer.....	53
6.5. Distinguishing HIFs from CTs.....	54
6.6. Testing Under Motor Loading.....	58
6.7. Testing Under HIFs with Shoulder .....	60
Chapter 7: Final Gatherings.....	61
7.1. Summary.....	61
7.2. Conclusions .....	62
7.3. Future Work .....	62
Appendix A: Measuring three-phase power .....	64
Appendix B: Moment of inertia of a machine .....	66

Appendix C: Harmonic Phase-ANGLE Measurement in Simplorer® .....	67
Appendix D: Final schematic in Simplorer® .....	69
REFERENCES .....	70

## LIST OF FIGURES

Figure 1. Potential HIF Due to Tree-Limb Contact.....	2
Figure 2. Distribution feeder showing substation, recloser, sectionalizers (top) and load type and locations (bottom) .....	5
Figure 3. Simplorer's multi-domain capabilities ( <i>courtesy: Ansoft support</i> ) .....	10
Figure 4. FFT block in Simplorer outputs in-progress information for spectral analysis.....	11
Figure 5. Screen-shots of a Simplorer® schematic ( <i>courtesy: Ansoft support</i> ) .....	12
Figure 6. Per-phase schematic of distribution feeder .....	13
Figure 7. Schematic of induction machine connected to a three-phase source for testing purposes.....	16
Figure 8. Per-phase (T-model) equivalent for induction machines.....	16
Figure 9. Induction machine properties window showing values used.....	17
Figure 10. Step block used to step torque demand .....	18
Figure 11. Torque characteristics of induction motor .....	18
Figure 12. Starting characteristics of induction motor based on data shown in Figure 9.....	19
Figure 13. Motor performance at different speeds .....	20
Figure 14. Industrial heater (right) modeled for simulation with its faceplate (left) .....	21
Figure 15. Electric heater model.....	22
Figure 16. Three-phase transformer part and its properties dialog .....	23
Figure 17. Test transformer circuit.....	24
Figure 18. HIF model using two time-varying resistances (left: KEPCO's EMTP model. Right: Simplorer®'s equivalent) .....	25
Figure 19. $R_2(t)$ value for shoulder (left) and non-shoulder (right) HIF cases. ....	26
Figure 20. V-I characteristic of $R_1(t)$ in the HIF model (left: KEPCO's result. right: implementation) .....	27
Figure 21 . Scaled down V-I curve for $R_1$ .....	28
Figure 22. HIF current showing build-up characteristics (left: shoulder case. right: non- shoulder case) (above: KEPCO's. bottom: implemented model) .....	28

Figure 23. $R_l$ 's Instantaneous and average resistance (left). Close-up showing highly non-linear resistance (right).....	29
Figure 24. Total instantaneous HIF impedance, $R1+R2$ showing highly non-linear behavior.	29
Figure 25. Steady-state HIF current waveforms.....	30
Figure 26. Current source mimics typical load demand.....	30
Figure 27. Comparison of a saturated CT waveform (top) and a HIF one (bottom).....	33
Figure 28. Modeling of a magnetizing branch to represent a saturable CT by means of an equation.....	35
Figure 29. Typical saturation curve of ferrite.....	35
Figure 30. Flux curves using equation 2 for multiple values of slope $\rho$ .....	37
Figure 31. Hysteresis loop parameters.....	38
Figure 32. Multiple saturable conditions showing hysteresis loops and their magnetizing currents based on equations 2 and 4.....	39
Figure 33. CT linear and saturated currents in steady-state (pu-Amps).....	40
Figure 34. Sample circuit to extract Fourier spectrum for saturable CT.....	40
Figure 35. Current spectra of saturated CT current. (top: actual spectrum. bottom: 1/f analog relationship).....	41
Figure 36. Comparison of hysteresis loops of a CT (top) and a HIF (bottom).....	42
Figure 37. Distribution feeder showing HIF disturbance points.....	44
Figure 38. Sectionalizer HIF-declare algorithm.....	45
Figure 39. Loading power demand phasors.....	48
Figure 40. Harmonic color-coding based on standard resistor colors.....	49
Figure 41. Fault after S1.....	50
Figure 42. Fault after S2.....	52
Figure 43. Fault after S3.....	53
Figure 44. Sectionalizer readings for a saturated CT for saturation level $\rho=30, b=0.05, a=40$ ..	55
Figure 45. Sectionalizer readings for a saturated CT for saturation level $\rho=15, b=0.3, a=40$ ....	56
Figure 46. Sectionalizer readings for a saturated CT for saturation level $\rho=28, b=0.15, a=40$ .	57
Figure 47. Schematic representation of HIF algorithm being tested against abrupt motor loading.....	58
Figure 48. Motor response under abrupt loading at $t=1s$ .....	59
Figure 49. Shoulder-present HIF harmonic-phase analysis.....	60

## LIST OF TABLES

Table 1. Typical HIF current values for fallen conductors.....	3
Table 2. Summary of some other work in HIF detection .....	9
Table 3. Common uses for Simplorer®.....	12
Table 4. Distribution feeder loads and elements .....	13
Table 5. Distribution feeder's segment impedance .....	15
Table 6. Induction machine rated faceplate information.....	17
Table 7. Dayton heater faceplate information.....	21
Table 8. Transformer element values.....	24
Table 9. Signature characteristics of HIFs .....	25
Table 10. Follow-through table showing how accurate a phasor can be measured .....	43
Table 11. Typical HIF current values for <15kV distribution feeders.....	46

# Chapter 1: High-Impedance Faults

## 1.1. Introduction

Distribution feeder conductor's are prone to physical contact with neighboring objects such as overgrown vegetation, building walls, or any surfaces below them. This condition raises the electric potential of tangible objects around us and may result in death by electrocution, severe electrical burns, or fires ignited by arcing and heating of materials. The occurrence of such conditions also constitutes a loss of energy to the power companies as not all of the produced electrical power is delivered to their appointed loads.

Power is lost on the way of delivery and dissipated through foreign objects which should not be in contact with the line. Conventional relaying schemes monitor short-circuit conditions where a significant amount of the energy supplied by the power company flows directly into the ground and never reaches its load. This condition is more critical for normal system operation than the one in this study. Diverse and effective solutions have already been found for this type of fault. The type of faulted condition in this study is the one that appears "invisible" to conventional fault detection methods and is caused by a leakage or small current that flows through surrounding objects that present high impedance in the current path to ground. These kinds of faults are hard to detect by monitoring equipment because their presence result only slight increases in load current; thus can be confused with a normal increase in load.

In this thesis a new technique is proposed to model, locate, and detect high-impedance faults. Patterns and characteristics in the line's current provide for recognition and are investigated to detect such faults. The characteristics of the line's current are referred to as *signatures* pertaining to a HIF and are used to derive an algorithm to detect the occurrence of such.

## 1.2. *Statement of Problem*

High-impedance faults (HIFs) are defined as unwanted electrical contact between a bare-energized conductor and a non-conducting foreign object. Non-conductors present high impedances to current flow due to their material, so a fault of this type will not appear to the protection equipment as an abnormal condition. Regardless of the circumstance of contact, a leakage current leaves the energized conductor and flows into the ground via tangible objects that are raised to a high potential posing a threat on human lives to say the least.

Foreign objects, in the case of study, are naturally non-conductors but may conduct if the applied voltage is sufficient. These foreign objects present high electrical impedances allowing only small amounts of currents through them. The most common type of high-impedance faults are caused when contact with tree limbs, vegetation, concrete walls, and ground surfaces occur. The aforementioned objects happen to be very close to the distribution feeder's conductors and are eligible for unwanted contact at any time. An outdoor distribution feeder shows the case of a potential tree-limb contact in Figure 1.

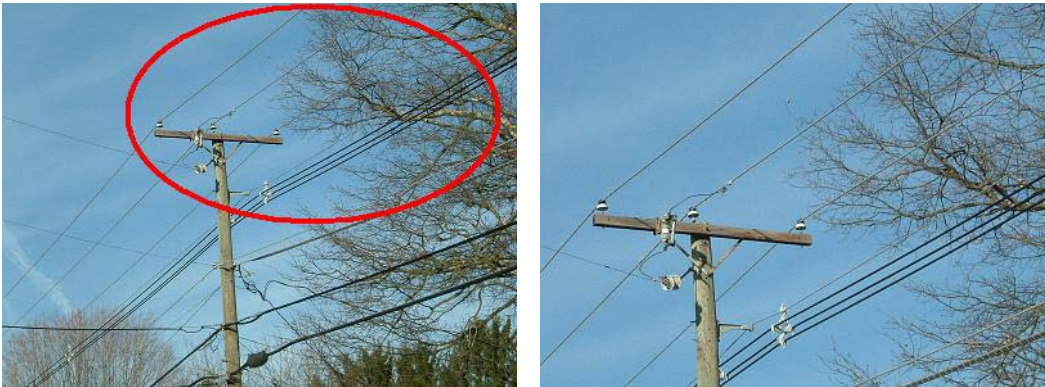


Figure 1. Potential HIF Due to Tree-Limb Contact

Conventional detection schemes monitor only low-impedance faults (LIFs that result in instantaneous and large increments of current due to a low-impedance path to ground (short-circuit). A HIF seems invisible to such detection methods because it presents only a small increment in line current and appears to be a normal load increment.

### 1.3. Purpose of Study

In lieu of public safety, energy conservation, and better electric service for consumers, a realistic model of a HIF is implemented and a method of detecting high-impedance faults is proposed. Conventional detection schemes “see” this problem as invisible, so even in its presence no alert or proactive action is ever taken.

In this work, two types of HIFs will be modeled and studied. The first is caused when an energized conductor breaks and falls onto the ground. This leaves the fallen conductor on the floor energized at its full potential but detached from the rest of the network. The contacting surface becomes a load to the broken phase end, and depending on the type of material, a variable amount of current may flow through it and into the ground. The current through such fault is small when the new path to ground presents high electrical impedance to current flow. Typical HIF currents values of this type [9] for a 12.5-kV distribution feeder are listed in Table 1.

MATERIAL	CURRENT (AMPS)
Dry asphalt	0
Concrete (non-reinforced)	0
Dry sand	0
Wet sand	15
Dry sod	20
Dry grass	25
Wet sod	40
Wet grass	50
Concrete reinforced	75

Table 1. Typical HIF current values for fallen conductors

The second type of HIF under consideration is the physical contact of a conductor with a neighboring objects when the conductor is fully energized, connected to the network, and supplying its load. This HIF condition appears to the monitoring equipment as a small increase in load current as seen in Table 1. For a conventional protection device an increase in

load current between 0 and 100-Amps can be either a HIF condition or an increase in load demand. There is no way to differentiate between load and HIF unless other patterns in the current waveform, besides amplitude, are identified. This leads to decomposing the line current into its spectral content and studying its harmonic content.

Not all HIFs can be represented by a single model, but certainly a number of HIFs behave in the same way. Most studies on HIF fault have been performed with test data from actual downed conductors [T&M],[KEPCO]. Due to the lack of these facilities at Virginia Tech the study of HIF required and accurate modeling of a HIF based on the available actual test data. This work takes an experimental model for HIFs proposed by Korean Electrical Power Company (KEPCO), a Korean utility company that has research experience in HIFs and has performed staged faults on their own distribution systems [10]. Besides from finding patterns in the current waveform, the proposed method takes advantage of the availability of communication functions in modern recloser and sectionalizer systems. This communication is assumed to be readily available from previous research conducted at Virginia Tech [11], and it is based on recloser-sectionalizer schemes that implement TCP/IP communication to isolate low-impedance faults. Hence, observations are made at different sections of the line and compared to each other to determine the fault location.

In the proposed method sectionalizers will determine unusual patterns in the line-current spectral component and it will be shown that harmonic phase analysis can be used as criteria for HIF detection. A one-line diagram representing the modeled system is shown in Figure 2.

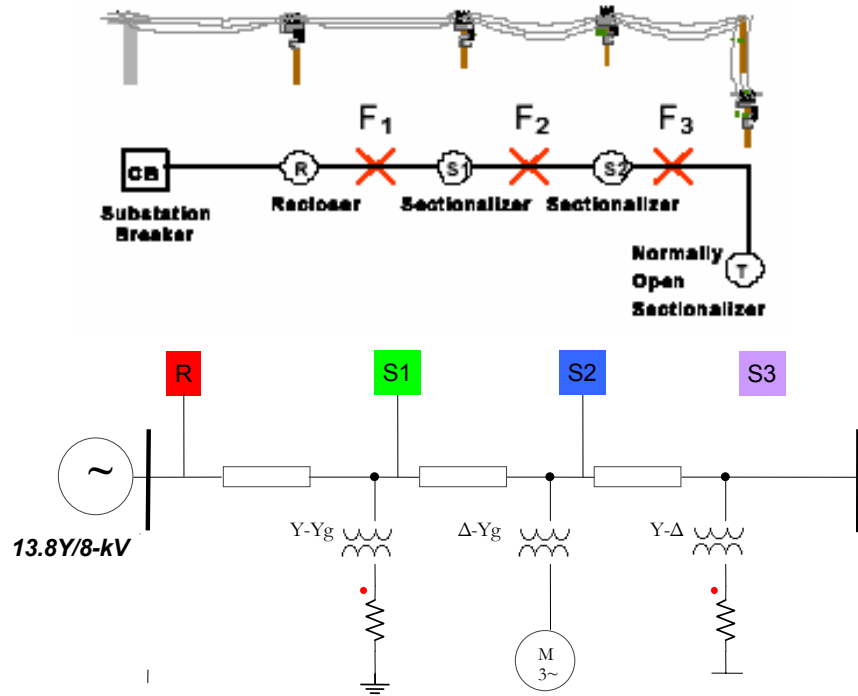


Figure 2. Distribution feeder showing substation, recloser, sectionalizers (top) and load type and locations (bottom)

In this study a HIF disturbances will be placed at F1, F2, and F3 respectively as line-to-ground fault. The captured harmonic information is used to test the proposed HIF detection and location algorithm.

The action of either alerting or isolating the fault is beyond the scope of this work. It involves liability issues and further urban/rural information must be considered before taking action. For instance, if a HIF exists due to a downed conductor near a school where children are exposed to the energized conductor, the action should be proactive the line should be tripped. On the other hand, if the same HIF occurs out in valleys where no habitat exists, the line should continue to distribute electrical service to its appointed pre-fault-location loads.

## **1.4. Other Work in This Area**

A restriction compromised by today's relaying schemes is that HIFs cannot be detected by an increase in load current alone. Other criteria has been explored and used as flags for detection to feed microprocessors. These other criteria are based on a spectral decomposition of the phase currents. The greater majority of HIFs occur on a single phase, thus each phase's current information is sampled and evaluated individually.

Researchers at Texas A&M University (TAMU) are pioneers in HIF detection and have investigated the problem since the early 80s. They were the first to license a commercial product to utility companies for HIF detection, but it must be remember that not all HIFs can be detected yet due to their highly random behavior, occurrence, and period of disturbance. A great number of HIFs can be detected today, but not localized due to lack of communication among distribution feeder sections, something that Virginia Tech intends on contributing to HIF detection by means of this and subsequent work. Other researchers have also investigated HIFs in depth and document their results; all which have something in common – the use of spectral decomposition to declare the presence of a HIF.

Among past HIF works published through the IEEE, it is documented that the fault current harmonics are a function of the system voltage and not of the load current. The phasor changes of the 3<sup>rd</sup> harmonic are measured in addition to its magnitude or phase position. High-impedance faults are inherently non-linear and always result in distorted currents, so harmonic analysis is critical in the evaluation and determination of HIFs. Phase information in the harmonics is shown to be significant in evaluating if a HIF exists. These fault harmonics are related to the system voltage at the point of fault, thus the lower the harmonic the more accurate and frequent its phase can be determined (i.e.  $1\text{ms} = 64.8^\circ$  for the 3<sup>rd</sup> harmonic while  $1\text{ms} = 151^\circ$  for the 7<sup>th</sup> harmonic at a sampling rate of 1-kHz). This is in part the reason why lower spectral components are preferred for HIF measurement. Also, the 3<sup>rd</sup> harmonic is a good measurement factor since it's the least disturbed by a resonant condition. A signature of a HIF, as described in [12] can be detected by 1) the change in the ambient 3<sup>rd</sup> harmonic current magnitude and 2) its relative phase to the system voltage.

In other work, researchers from TAMU [13] developed algorithms based on current magnitudes and waveforms. A variety of algorithms to assess a HIF are implemented, but only two are detailed and described in some depth. The *energy algorithm* detects sudden changes in energy for a certain harmonic group as indicative of the presence of an arcing fault. The *randomness algorithm* looks for highly sporadic behavior or rapidly changing dynamic characteristics of the faulted-phase current waveform and detects a broken or contacting conductor (detects a loss of load prior to arcing).

The detection logic used by their microprocessors uses two (or more) algorithms for analyzing four currents (3 phases + neutral) and their three spectral groups (odd, even, and none). A total of 24 inputs are taken into the microprocessor to determine a HIF ( $2 \times 4 \times 3 = 24$ ). Timers are intended to rule out normal system activity such as bank switching, motor starting, or load shifting. It is considered that nominal systems disturbances such as the aforementioned are occasional and momentarily only. High-impedance faults must be detected within the first minute of occurrence, otherwise due to changing media conditions (chemical properties in lieu of heat, and ionization) they never will be detected since the current may level off to normal again (while the HIF still exists).

When the pre-programmed logic believes there's a HIF, the system's alarm state changes. If the confidence level reaches 100% (first presence of a HIF), the algorithm resets the flags and tests the system all over again. If the HIF still exists, and the second confidence level is again acceptable (i.e. >80% of confidence), it tries one last time. If the detection is again acceptable again, an alarm triggers. This system was developed by Texas A&M Power System Automation Laboratory (PSAL) and it is currently licensed to General Electric (GE). Ever since GE's acquisition of this product, HIF research de-intensified as the end-product detects a good number of HIFs today.

Researchers at the University of Milwaukee [14] modeled over 200 non-linear high-impedance faults using the Electro-Magnetic Transients Program (EMTP), a computer based power systems software known reliable for its accurate results and transient accuracy. Their algorithm logic analyses, in five-minute intervals, load and negative sequence currents for incremental changes (~20%) to determine candidacy of a HIF. The magnitude of the 3<sup>rd</sup> and 5<sup>th</sup> harmonic currents discriminate against regular switching, inrush currents, and a highly non-

linear fault impedance. Also, the percent increase in 3<sup>rd</sup> harmonic current with respect to line current ( $i_3/i_1$  ratio) triggers a flag. The suggested logic in [14] meant for HIFs can also be applied for LIFs with little modification. A system that detects both HIF and LIFs is proposed in [14] as a better and more effective solution, but it must be noted that all measurements are made at a virtual substation simulated in EMTP and solutions presented in real life would require a power engineer's intervention at the control house. The referred work also shows studies of downed vs. broken-down conductors performed by comparing amount of non-linearities in the faulted currents. A sustained incremental change of angle between 3<sup>rd</sup> current with respect to phase voltage (taken at  $\varphi_v=3\pi/4$  as the voltage phase reference) determines abnormal circumstances. If any (OR-gate) phase triggers all (AND-gate) five detection flags (load current, negative sequence current, 3<sup>rd</sup> harmonic angle, 3<sup>rd</sup> and 5<sup>th</sup> harmonic current magnitudes) the timer starts before it triggers the alert. From the above summarized work, it is seen that spectral analysis is required from every HIF algorithm. This implies a powerful enough microprocessors based detection schemes performs limited spectral analysis of the signal. The above mentioned works and their requirements for algorithm implementation are summarized in Table 2.

Authors	Institution	Line Current Information Needed	Spectral Range Needed	Detects
[12] C. Benner D. Russell	Texas A&M	Angle between 3 <sup>rd</sup> harmonic and system voltage	180 Hz	HIFs
[13] D. Jeerings R. Linders	Nordon R&D	3 <sup>rd</sup> harmonic magnitude and angle with respect to system voltage	180 Hz	HIFs
[14] D. Yu S. Khan	University of Wisconsin – Milwaukee	3 <sup>rd</sup> , 5 <sup>th</sup> , 7 <sup>th</sup> , neg.seq. current, angles between 3 <sup>rd</sup> and 5 <sup>th</sup> , 3 <sup>rd</sup> and system voltage.	60 – 500 Hz	HIFs, LIFs, arcing HIFs, broken or downed conductors

Table 2. Summary of some other work in HIF detection

[#]=reference number

What has not been documented yet is the localization of such HIFs – only their detection criteria. All documented work in this area of HIFs makes measurements and base their results as seen from substations and do not communicate their observations to other sections to localize the HIF.

This work combines HIF detection criteria together with internet-based sectionalizer-recloser technology to not only detect HIFs, but also to localize the faulted point as illustrated by Figure 2.

## Chapter 2: Simulation Software

### 2.1. Ansoft Simplorer®

To investigate the patterns presented by HIFs, computer software is chosen as preferred to physical system testing. The use of simulations allows for line-current spectral analysis at any desired sampling rate, and makes adding or changing load scenarios trivial. Ansoft Simplorer® version 6.0 (2002), one of the industry's leading circuit simulation software, is chosen. Simplorer® is a complete and powerful electrical engineering simulation software that has the ability of modeling many types of electric and electromechanical systems. It incorporates circuitual parts from various areas of electrical engineering, including semiconductors, power electronics, digital signal processing, controls, power systems, machines, converters, drives, etc. Simplorer® is also a multi-platform and multi-domain simulation software. It allows results from any of the domains of electric, fluid, magnetic, mechanical, or thermal results to combine and processes together as shown in Figure 3.

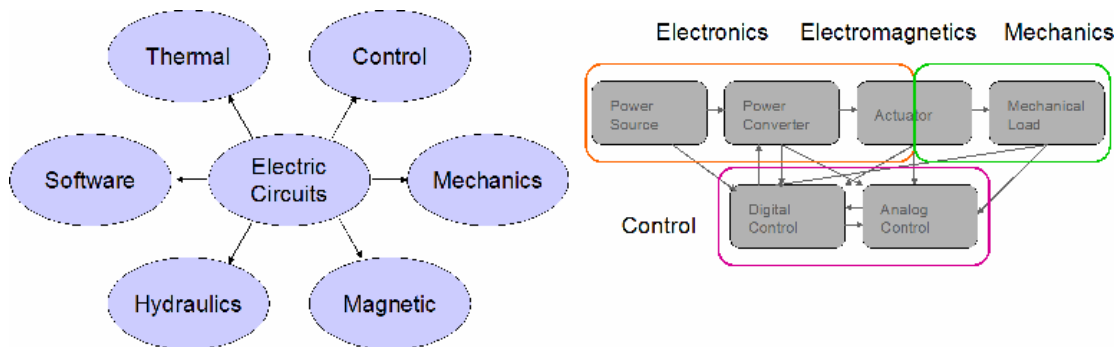


Figure 3. Simplorer's multi-domain capabilities

*(courtesy: Ansoft support)*

Simplorer® uses fast and stable simulation algorithms that reduce design time and provide reliable results. In addition Simplorer® has a friendly user interface that allows the drag-and-drop of parts such as resistors, inductors, wires, machines, etc. It has hundreds of parts varying from semiconductors, transformers, machines, control blocks, prime-movers, state-

space, etc. that make it suffice to model any task. With these features it is easy to interconnect elements in a presentable format and obtain accurate results.

All parts modeled by Simplorer® can be combined to build even more realistic models. For instance, a three-phase power meter is not available, but by combining two instantaneous wattmeters and sliding-mean blocks, the total three-phase power can be obtained (see Appendix A). As another example, it is possible to make accurate harmonic-phase measurements at the sampling frequency desired (i.e. 1kHz, 2kHz, 8kHz, 10kHz) by using the real-time fast Fourier transform (FFT) block. This block outputs real-time (i.e. dynamic, online, or in-progress) frequency, amplitude, and phase information of spectral content given an input signal (i.e. a non-linear voltage or current). This function is key in the study of HIFs and it is one of the main reasons why Simplorer® was chosen over its other counterparts such as PSpice®. A use of the FFT block showing the part is shown in Figure 4.

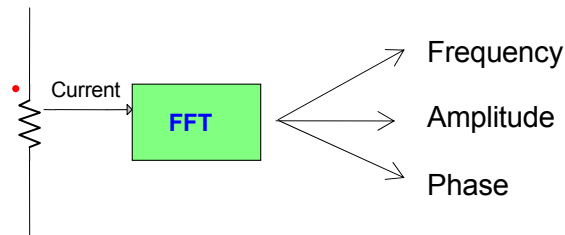


Figure 4. FFT block in Simplorer outputs in-progress information for spectral analysis

The tools and parts that Simplorer® comes bundled with suffice to model any electrical network. There are practically no limitations as what can be modeled. A list of typical uses for Simplorer® is shown in Table 2.

APPLICATION
AC / DC motor drives
Switching power converters/inverters
Automotive electrical systems
Transient studies in electronic circuits
Controls and feedback systems
State space modeling
Electronics
Thermal analysis
Mechanical loading

Table 3. Common uses for Simplorer®

A screen-shot showing Simplorer®'s friendly user interface is shown in Figure 5

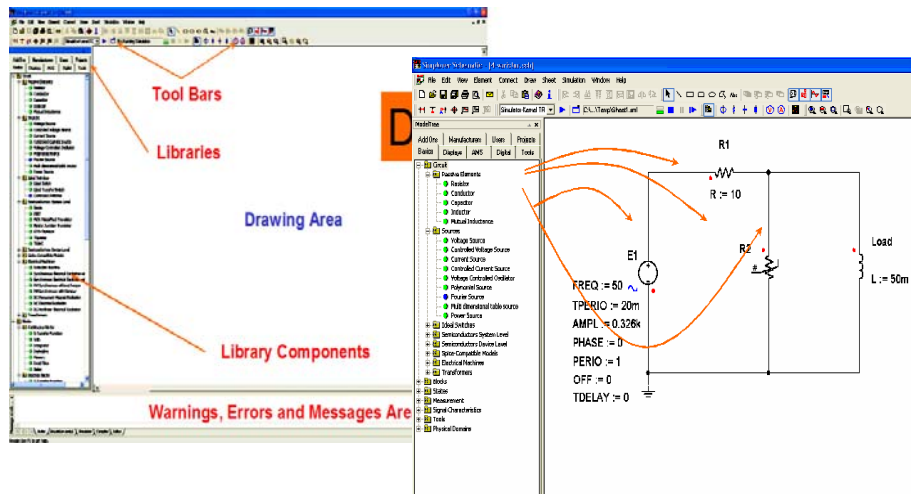


Figure 5. Screen-shots of a Simplorer® schematic  
(courtesy: Ansoft support)

Realistically, line measurements are based on voltage and current transformer (CT) readings. Should a CT saturate for any reason, the readings provided to the measuring equipment will be incorrect and false alerting or triggering may occur. To account for this effect, a model for a saturable CT is needed to observe the line currents during saturation. Simplorer® does not have a saturable-core based transformer model; neither for voltage or current. The transformers in Simplorer® are ideal and of infinite performance, so the simulations are limited to linear-region and steady-state operating points.

## Chapter 3: Electrical Load Models

### 3.1. Distribution Feeder

The system modeled selected for this study consists of a 13.8-kV distribution feeder of ~20 miles in length. It is formed by three sections of equal length and equal segment impedance. Each segment carries one load behind its appropriate and ideal step-down phase transformers. The loads are of different types and behind different kinds of transformer banks. A summary of the distribution feeder in study is shown in Table 4. A per-phase schematic representing the elements shown in Table is shown in Figure 6

ELEMENT	QUANTITY
Generation / Source	3 $\phi$ , 13.8Y/8-kV, four-wire
Line impedance	3 R-L sections
Phase transformers	3 ideal step-downs of 13800:460V $\Delta$ -Y <sub>g</sub> , Y-Y <sub>g</sub> , and Y- $\Delta$ connected banks
R-type load	2 industrial heaters (Y <sub>g</sub> and $\Delta$ connected)
L-type load	1 induction machine (150hp)

Table 4. Distribution feeder loads and elements

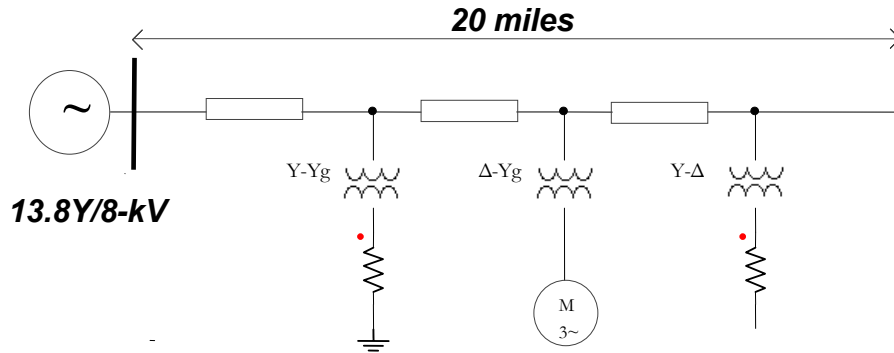


Figure 6. Per-phase schematic of distribution feeder

### 3.2. Transmission Cables

In a distribution feeder of 20 miles in length, the shunt capacitance can be neglected entirely without much loss of accuracy [2], and a line can be modeled with only series  $R$ - $X$  losses. Simplorer® comes with a 1 $\phi$  per-meter lossy transmission line model, but it was not used as its shunt elements (capacitance and conductance) can be neglected. To connect the loads, the line was tapped at equidistant segments of  $\sim 20/3^{\text{rd}}$ s of a mile. The inductance per line segment depends only on the conductor size and spacing [3]. The spacing  $d_{mean}$  is taken as the geometric-mean separation of the three phase conductors, thus given by

$$d_{mean} = \sqrt[3]{d_{12}d_{23}d_{31}} \quad < m >$$

where  $d_{ij}$  is the separation, in meters, between conductors  $i$  and  $j$ . Knowing the mean conductor separation  $d_{mean}$  the inductance per meter is

$$L = \frac{\mu_0}{8\pi} \left( 1 + 4 \ln \left( \frac{d_{mean}}{r} \right) \right) \quad < H / m >$$

where  $r$  is the radius of each phase conductor. Using an inter-conductor spacing of  $d_{ij}=1\text{m}$ , segment length of  $\sim 11$  km ( $\sim 20/3$  miles), a conductor radius of  $r=2\text{cm}$  yields a per-meter inductance of

$$L = \frac{4\pi \times 10^{-7}}{8\pi} \left( 1 + 4 \ln \left( \frac{1}{0.02} \right) \right) = 832\text{nH} / m$$

From this result, the appropriate reactance per segment can then be found. The segment resistance is chosen to be  $0.5\text{-}\Omega$  as a standard value for the modeled conductor size and length. A summary of the segment impedances is shown in Table 5.

ELEMENT	VALUE
Segment resistance, $R_{seg}$	0.5 $\Omega$
Segment inductance, $L_{seg}$	9.15 mH
Segment reactance, $X_{seg}$	3.44 $\Omega$
Number of Segments	3
Per-meter inductance, $L_{pm}$	832 nH
Per-meter reactance, $X_{pm}$	313 $\mu\Omega$
Conductor radius, $r$	2 cm

Table 5. Distribution feeder's segment impedance

### 3.3. Induction Motor

Between 60 and 70% of the electric energy produced in the United States is consumed by electric motors [15], therefore it is important to model a motor in the distribution feeder. An induction motor is modeled because it is a widely used industrial machine and has large starting currents that alter the current characteristics of the line momentarily. Synchronous motors when being started also present this characteristic because they are momentarily re-configured, by shorting out the rotor, to turn them into induction motors for starting purposes. Therefore, a full-time induction motor is a good choice because it can represent either a synchronous or induction motor during startup without having to re-configure its rotor windings.

Simplorer® has a Y-connected, squirrel-cage wound rotor, three-phase induction machine model [8] as an available part. This avoids the need of creating a model for a machine using analog behavioral blocks or transfer functions and is another reason why Simplorer® was chosen over PSpice®, the popular electronic-circuit simulation software. To test the machine's performance, a model was taken from [7] and simulated to obtain curves for torque, speed, horsepower, and efficiency. The machine was first connected as shown in Figure 7 and two wattmeters were used to extract the three-phase power as explained in Appendix A.

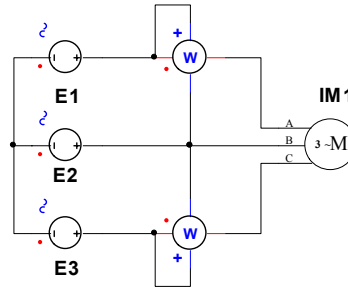


Figure 7. Schematic of induction machine connected to a three-phase source for testing purposes

In typical power simulation software, an induction machine is modeled by specifying its VA rating, line voltage, and percent impedance. In Simplorer®, the machine's parameters are entered manually according to the T-model [7]. The per-phase equivalent (or T-model) that Simplorer® uses is shown in Figure 8.

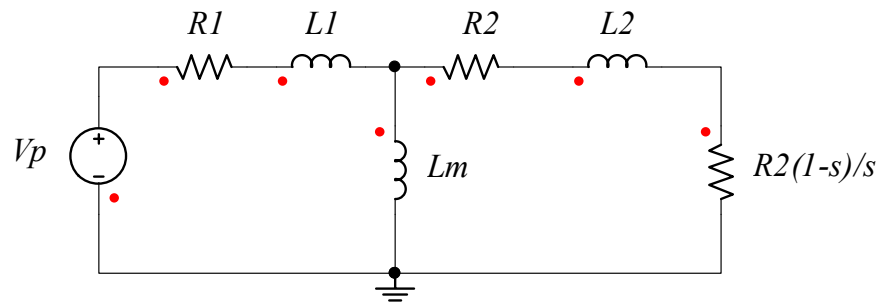


Figure 8. Per-phase (T-model) equivalent for induction machines

To model a realistic machine, an example was taken from [7] and the values input to Simplorer®. The machine properties window is shown in Figure 9 showing how the data values entered.

Parameters (Value, Variable, Expression)	
Name	Value
Load Torque [Nm]	0
Stator Resistance [Ohm]	0.087
Rotor Resistance [Ohm]	0.228
Stator Leakage Inductance [H]	(0.302/377)
Rotor Leakage Inductance [H]	(0.302/377)
Main Inductance [H]	(13.08/377)
Number Of Pole Pairs	2
Moment Of Inertia [kg*m <sup>2</sup> ]	1.662

Figure 9. Induction machine properties window showing values used

For more information about the moment of inertia of a machine (last item in Figure 9), refer to Appendix B. The information given above approximates an industrial machine of rated faceplate information as shown in Table 6, a rotor of about 10-kg, and a radius of 57-cm.

CHARACTERISTICS	VALUE
Line Voltage	460 V
Horsepower	150 hp
Torque	800 N-m / 590 ft-lbf
Speed	1800 rpm
Pole Pairs	2

Table 6. Induction machine rated faceplate information

Given the T-model and parameters shown in Figure 9, the machine's performance was captured and is shown in Figs.11-13. During steady-operation, the machine turned at 1750-rpm moving a load of 150-N-m. The induction machine is not ran at rated conditions, but at typical ones instead thus maintaining its efficiency >80%. For the different loads that could have specified in N-m, the machine can operate at different efficiencies. The decision of operating at high efficiency was preferred over operating at rated torque.

Simplorer® allows for the torque on the induction machine to be stepped at any time during the simulation using the step-block as shown in Figure 10

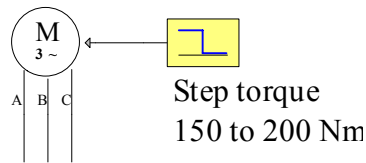


Figure 10. Step block used to step torque demand

This permits to see how the line current behaves when machines have an abrupt change in their load. The HIF algorithms developed later will have to detect this condition and ignore it as its normal load behavior. Initially the machine was ran unloaded until steady-state was reached (no value for load torque was specified). At a later point in time, its load torque will be stepped to show that it will not affect our results in finding HIFs. The torque vs. speed characteristics of the motor are shown in Figure 11.

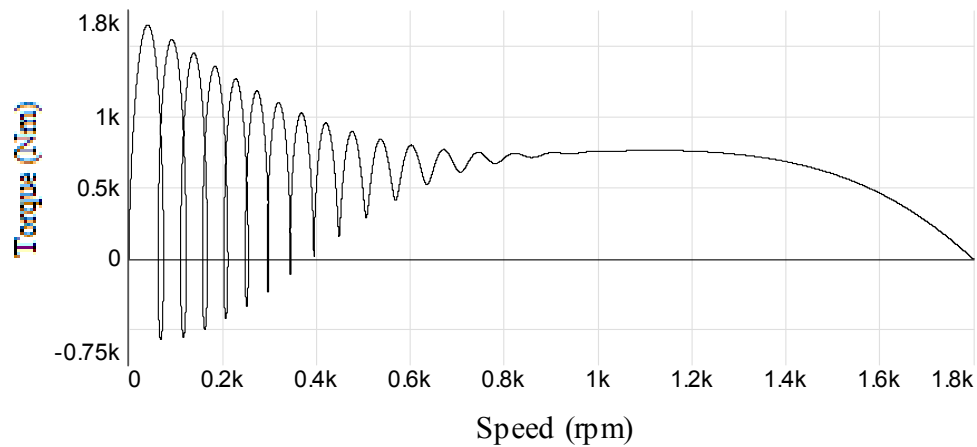


Figure 11. Torque characteristics of induction motor

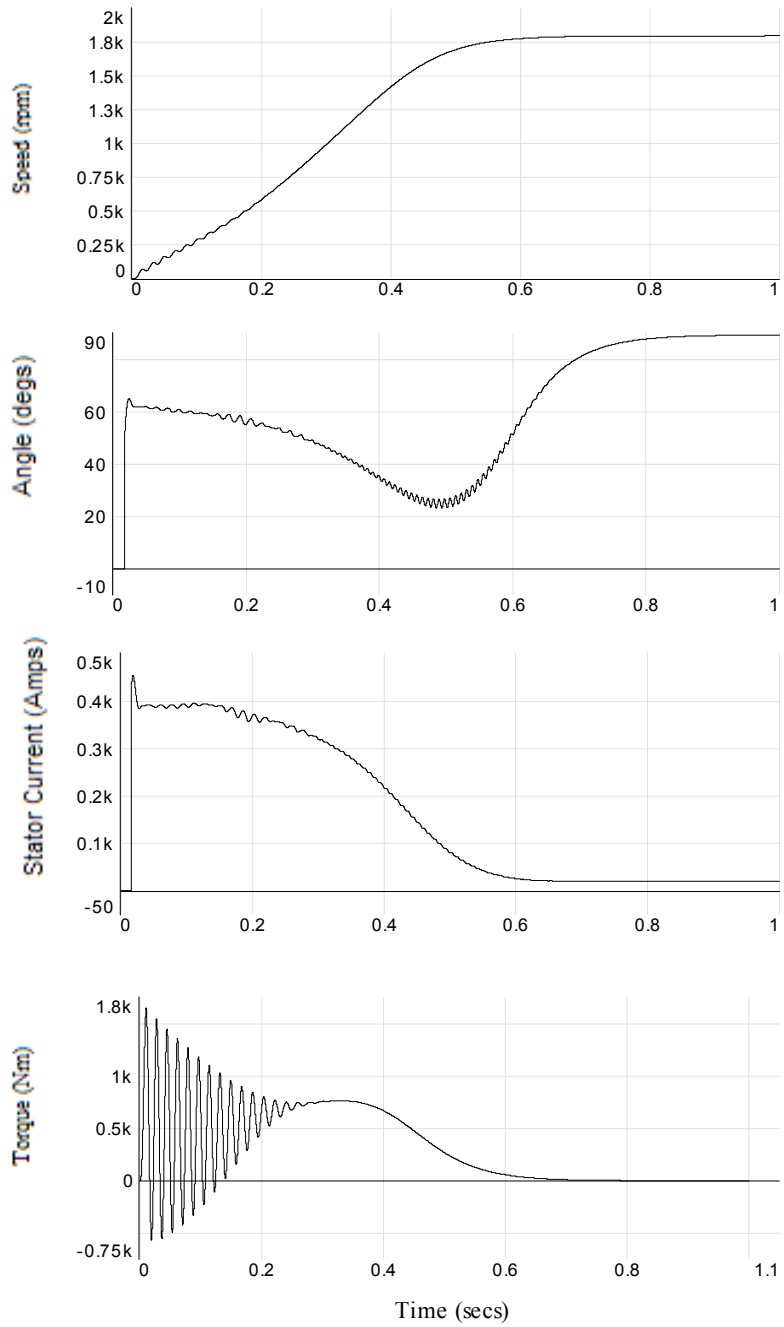


Figure 12. Starting characteristics of induction motor based on data shown in Figure 9.

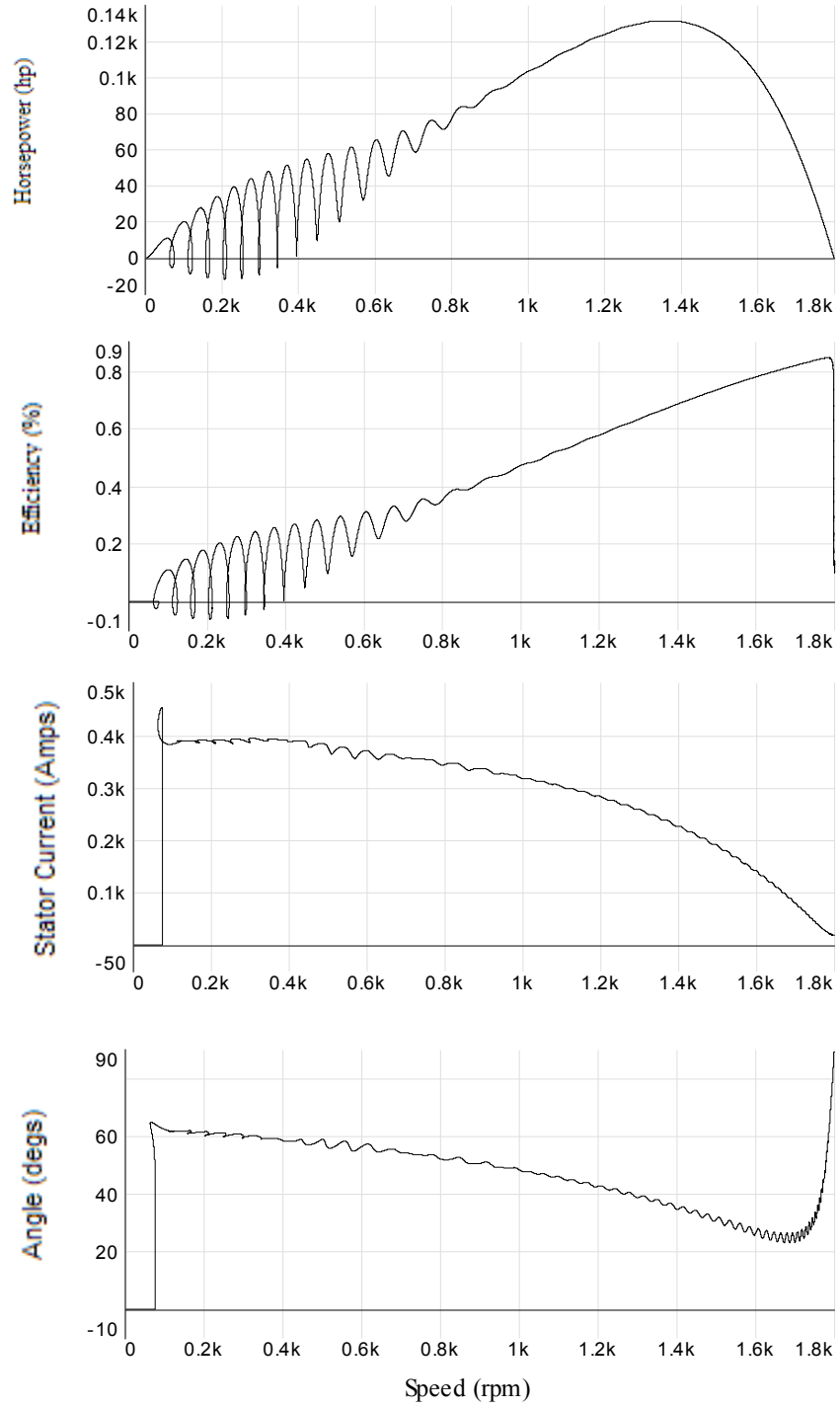


Figure 13. Motor performance at different speeds

### 3.4. Industrial Heater

An industrial heater is modeled as a resistive load. A model for this load is put together by taking the faceplate data and replicating the power consumption. A picture of a 30-kW Dayton electric heater model is shown in Figure 14



Figure 14. Industrial heater (right) modeled for simulation with its faceplate (left)

The faceplate information is shown below and copied in Table 7 for clarity.

MODEL	3E192
WATTS	30,000
PHASE	3
AMPS	83.4
MIN.CIRCUIT AMPS	85.4
MAX.PROTECTIVE DEVICE AMPS	110
MOTOR AMPS	2.00
MOTOR VOLTS	208
HEATER VOLTS	208

Table 7. Dayton heater faceplate information

Assuming the heater to be completely resistive, the per-phase impedance is found from the given faceplate as

$$R = \frac{V^2}{P} = \frac{208^2}{30000} = 1.44\Omega$$

The electric heater 3 $\phi$  model is constructed in Simplorer® and shown in Figure 15

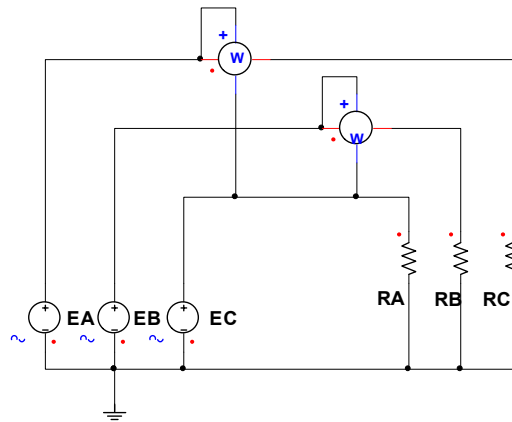


Figure 15. Electric heater model

The two-wattmeter method (see Appendix A) measure 30-kW as the total power delivered to the load. This shows the model to be accurate as it agrees with the faceplate information in Figure 14. In Figure 15, the heater is connected in Y form, but a  $\Delta$  heater is also used as another R-type load during simulation.

### 3.5. Voltage Transformers

Simplorer® comes with a three-phase transformer model with appropriate coupling coefficient constants for its windings. The transformer model is linear and never saturates, as is also the case with real power transformers. Therefore, there was no need to derive a model for its non-linear core properties as is done for current transformers in the next chapter. The transformer part and its properties are shown in Figure 16.

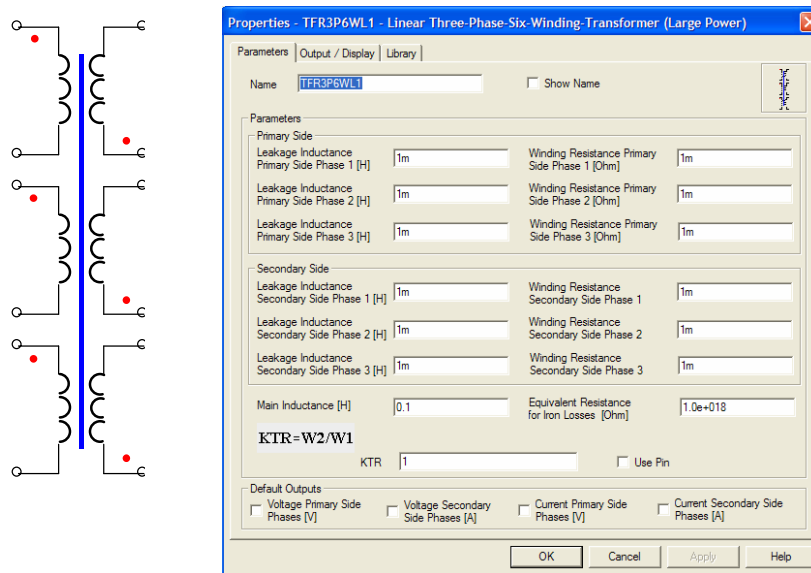


Figure 16. Three-phase transformer part and its properties dialog

The information required in the properties dialog on the right of Figure 16 is based on the classical per-phase transformer model, in which the primary and secondary resistances and leakage inductances must be specified. The magnetizing branch impedance must be specified in the form of its core ohmic-losses and main magnetizing inductance. Simplorer requires that transformers be specified in this fashion because this part is also available for electronic circuit designers, in which detailed information of the transformer is specified. In power systems, normally transformers are modeled as an in-line reactance followed by a set of windings, but not in Simplorer®. This is not a limitation because accurate data about transformers is available and can be found in textbooks.

For the 13.8-kV distribution feeder, the transformer data was taken from [5] and tested using the circuit shown in Figure 4.

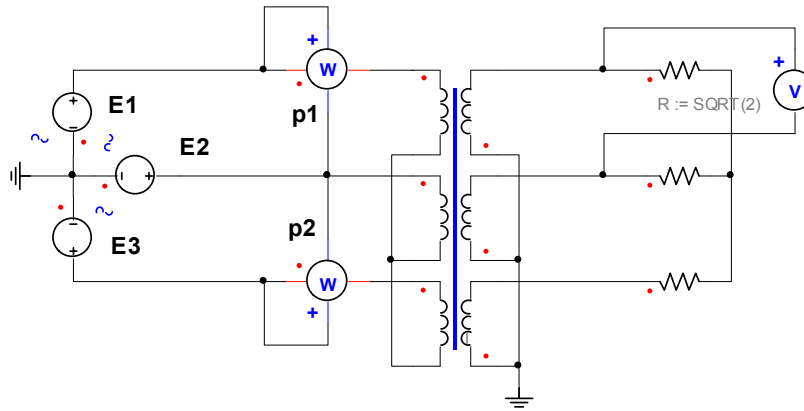


Figure 17. Test transformer circuit

The data input into the transformer is shown in Table 8.

ELEMENT	VALUE
Primary resistance	4 $\Omega$
Secondary resistance	0.04 $\Omega$
Primary leakage inductance / reactance	13.2 mH / 5 $\Omega$
Secondary leakage inductance / reactance	0.13 mH / 0.05 $\Omega$
Core losses	35 k $\Omega$
Main inductance / reactance	10.6 H / 4 k $\Omega$
Turns ratio ( $n_1/n_2$ )	13.8k/460 = 30

Table 8. Transformer element values

The transformer's VA capacity, since ideal, is infinite. This means that the transformer does not show unusual behavior due to overloading.

### 3.6. High-Impedance Fault Model

High-impedance faults have “signature” characteristics in their transient and steady-state regimes that make them identifiable. These characteristics are listed in Table 9. To simulate a HIF, the model is taken from [10] and reproduced in Simplorer® using two time-varying resistances. The two variable resistances cause the phase current to present the characteristics of Table 9.

SIGNATURE	DESCRIPTION
Asymmetry	HIF current presents DC offset making it asymmetrical
Build-up	HIF current progressively increases until it reaches steady-state.
Shoulder	During build-up HIF current halts increase for a few cycles then continues
Non-linearity	HIF current not truly sinusoidal. Pronounced odd harmonics

Table 9. Signature characteristics of HIFs

Not all HIFs present shoulder, but some do so both the no-shoulder and shoulder-present cases are modeled to cover a wider variety of HIFs in looking for consistent patterns. To reproduce the HIF model in Simplorer®, two resistances  $R_1$  and  $R_2$  are placed in series as shown in Figure 18.



Figure 18. HIF model using two time-varying resistances (left: KEPCO’s EMTP model. Right: Simplorer®’s equivalent)

The second resistance  $R_2$  decays exponentially reaching the value of zero after  $\sim 0.4$  seconds for the non-shoulder case, and  $\sim 0.5$  seconds for the shoulder case. This characteristics is what produces build-up.

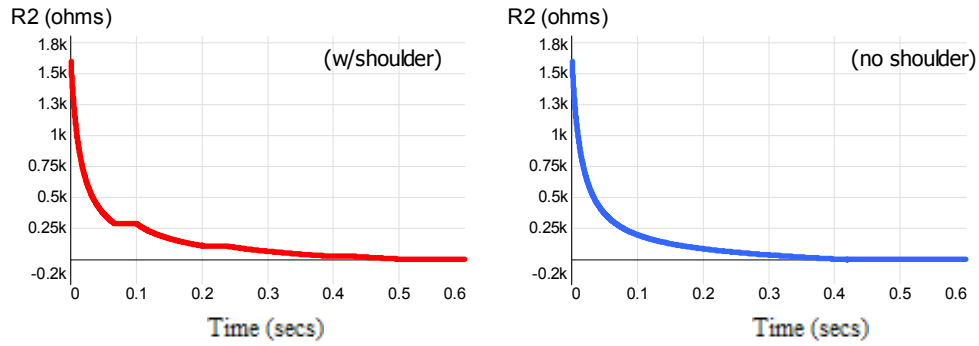


Figure 19.  $R_2(t)$  value for shoulder (left) and non-shoulder (right) HIF cases.

Two curves for  $R_2$ 's exponential decay are shown in Figure 19. The leftmost presents aperiodic flat slopes that cause the shoulder effect on the HIF current by maintaining the same value of resistance for small periods of time; this stops the current from increasing momentarily. The rightmost curve is the no-shoulder case and it causes a continuous exponential increase in HIF current. The equation for  $R_2(t)$  for the no-shoulder case is found by inspection from KEPCO's results in [10] as

$$R_2(t) = \frac{1600}{1 + 65t} - 135t$$

The first resistance  $R_1$  oscillates, non-linearly, about a  $200\text{-}\Omega$  for the  $\sim 20\text{-kV}$  per-phase feeder given in [10]. This produces non-linearity in the current waveform while maintaining a HIF impedance close to  $200\text{-}\Omega$  in steady-state. The V-I values for  $R_1$  were input in the form of data-pairs through Simplorer®'s ScanSheet tool. This tool allows inputting any curve in the form of data pairs by clicking points with the mouse. To verify that the model implemented was accurate, a comparison plot of the V-I characteristics of  $R_1$  are shown in Figure 20.

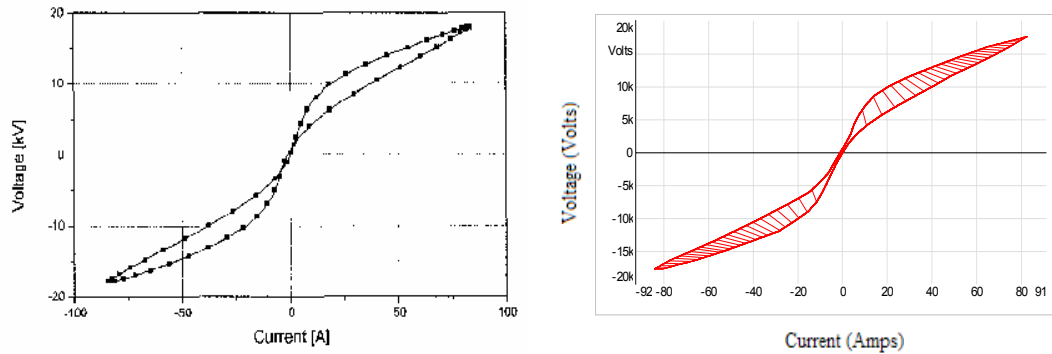


Figure 20. V-I characteristic of  $R_1(t)$  in the HIF model (left: KEPCO's result. right: implementation)

The results in Figure 20 show that the implemented HIF model is in agreement with KEPCO's. The V-I characteristics of  $R_1$  shown in Figure 20 show how the V/I ratio (instantaneous resistance) varies non-linearly. This introduces non-linearity and approximates a realistic a HIF condition. The rightmost V-I curve in Figure 20 is scaled down to fit the 13.8-kV feeder in study. The scaled down curve is shown in Figure 21 showing a per-phase voltage of 8-kV and maximum current of 40-A. It is scaled down by re-inputting the data pairs for  $R_1$  and specifying new limits for the V-I characteristics.

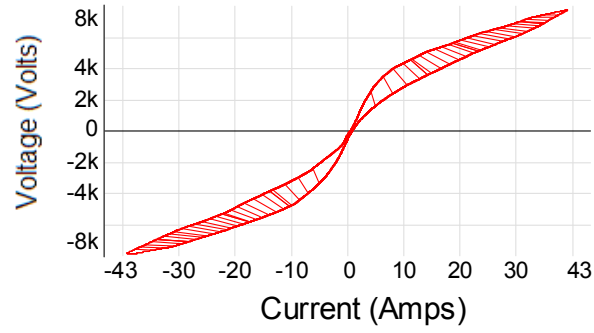


Figure 21 . Scaled down V-I curve for  $R_1$

The interlacing lines show how the differential voltage of  $R_1$  is increasing while  $R_2$  is decaying exponentially as mentioned before. The produced HIF build-up currents produced by  $R_1$  and  $R_2$  are shown in Figure 22.

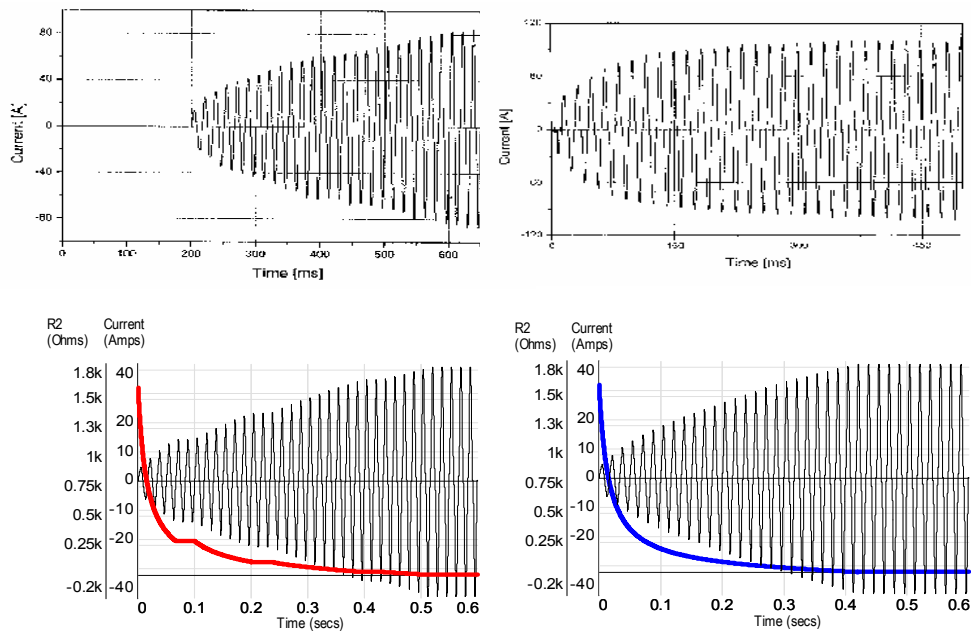


Figure 22. HIF current showing build-up characteristics (left: shoulder case. right: non-shoulder case) (above: KEPCO's. bottom: implemented model)

To show how the value for  $R_1$  changes while  $R_2$  decays, an instantaneous plot of its resistance is shown in Figure 23 along with its time-average value.

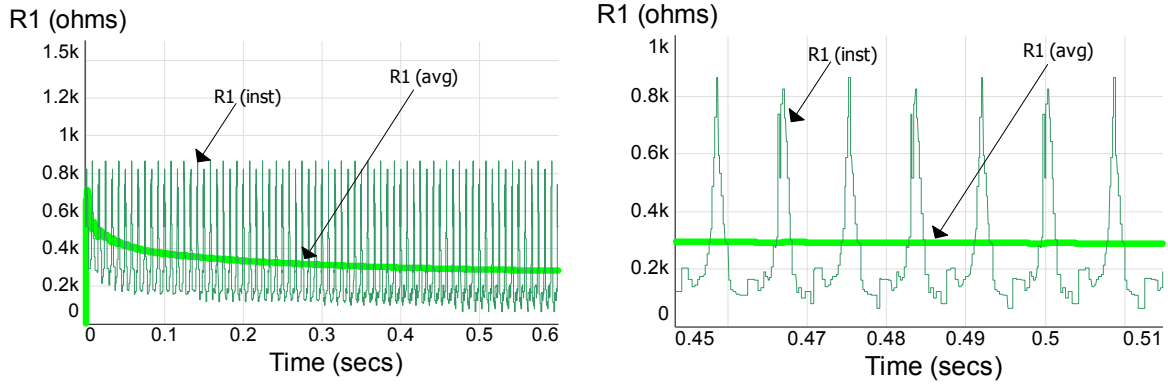


Figure 23.  $R_1$ 's Instantaneous and average resistance (left). Close-up showing highly non-linear resistance (right).

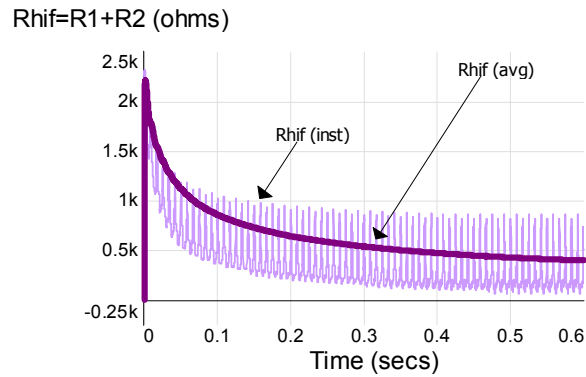


Figure 24. Total instantaneous HIF impedance,  $R_1+R_2$  showing highly non-linear behavior

The total HIF resistance  $R_{HIF}(t) = R_1(t) + R_2(t)$  is shown in Figure 24. The amplitude of the HIF current in Figure 22 falls in the typical range given in Table 1. The HIFs are placed in different sections of the distribution feeder and patterns as phase-to-ground or phase-to-phase faults.

In the steady-state regime, the HIF modeled implemented is shown to agree with the non-linear current characteristics of KEPCO’s model. Below are the comparison figures before scaling the V-I plot of Figure 20.

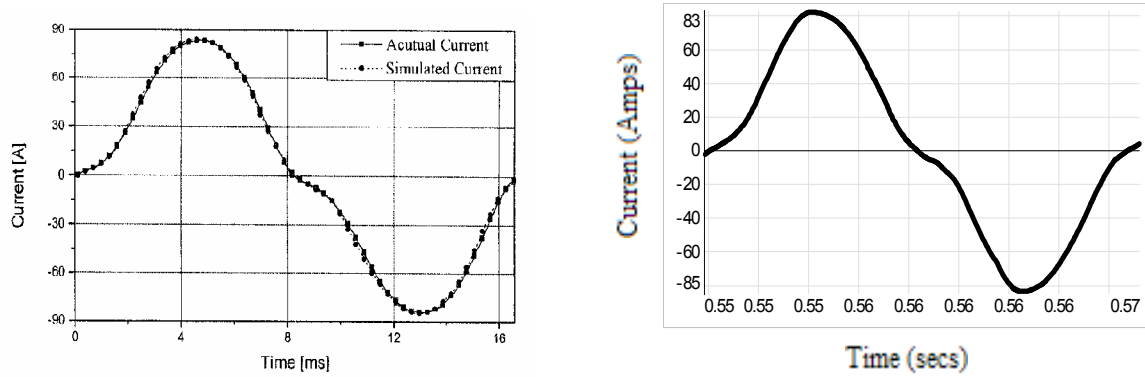


Figure 25. Steady-state HIF current waveforms

### 3.7. Summary of Modeled Loads

The loads were carefully chosen and modeled based on what is typical on a distribution feeder. The steady-state (motor unloaded) line current is about 50-A. This is rather low on a 20-mile distribution feeder, but the addition of more loads is not necessary because the proposed HIF algorithm works regardless of the loading conditions (i.e. for 50 or 500A line current). Yet, in order to simulate more loads on the line, current sources (one per phase) are placed at end of the bus to pull current (~500A) through the feeder and source “fictitious” loads behind the second bus. The idea of “fictitious loading” is shown in Figure 26 in a one-line diagram.

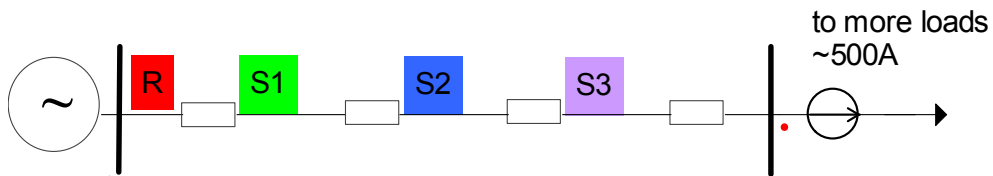


Figure 26. Current source mimics typical load demand

Distribution feeders don't present much transmission losses as it is. The voltage losses from one of the line to the other (from bus to bus, or from before R to past S3), should be less than 5%, meaning that no less than 13.1-kV is expected at the second bus. The use of fictitious loading increases the losses on the line (~500A causes larger voltage drops than 50A), so it should be noted that the line impedances are decreased manually when using the current source (R and L are reduced by a factor of 10).

Typical outdoor distribution feeders show single- or three-phase transformers on the wooden poles in the form of cylinders as in Figure 26. These are modeled with the phase transformers. They are considered ideal because they don't saturate; it would take an enormous (atypical for a distribution feeder) load current to saturate their core. The inter-coupling coefficients for the spiral-based transformer models are all accounted for in Simplorer®; the transformer needs no further adjustments and ready-to-use as they come.

The induction motor is an integral part of the distribution feeders. Machines of this type are used in pumps, compressors, fans, mills, elevators, etc. As mentioned before, the majority of the electrical loads are motors [15]. Not so much synchronous motors due to their rare applications and pricing, but more induction motors could have been used instead. If studying detailed transient effects of dynamic loads (i.e. a phase's voltage drop due to a LIF could cause the charged inductance of a motor to discharge towards the HIF "fooling" sectionalizer readings).

Industrial heaters are of importance as well. They are all around us and in large public places (i.e. shopping centers/malls, in-door pools, buildings, etc.). Heaters contribute a high percentage of real-power demand. Their low real-impedance demands high current which consumption is dissipated as heat ( $p=i^2r$ ). These types or loads are considered "static" loads, meaning that they are not dynamic and don't contribute, or are altered, due to disturbances in the distribution feeder.

The modeling of HIFs has always been a challenge. There is no one correct model for all HIFs nor one that will adjust itself to model the properties of soil or material due to electrical burning, heating, or arcing. High-impedance faults are typically studied by staged-faults [10], [13] instead of electrical modeling. The reason being is that observations captured from real-

life acquisitions better serve the purpose of finding typical patterns in the current waveforms. Some believe that modeling HIFs electrically with computer simulation programs such as EMPT® can be more efficient [14] and cover a wider range of scenarios. This is true when many HIFs models are available because an overall typical pattern can be found. This eliminates the need for downing or breaking conductors every time an algorithm or a variation of scenarios needs to be tested.

The study in this work is based on an electrical HIF model documented by KEPCO, an electrical utility company in Korea. They, from staging faults on their own distribution feeders, have produced a model that aids them in modeling HIFs in EMTP. This is also the idea behind [14] and the one adopted in this thesis; the modeling, detection, and localization of HIFs based on electrical models.

## Chapter 4: Modeling of Saturable Current Transformers (CTs)

### 4.1. The Need for Modeling CTs

In distribution feeders, current transformers (CTs) might reach momentary saturation due to large motor starting-currents, short-circuit conditions, burden faults, or an excess demand in one of their phases. The pronounced third-harmonic current, and its angle, in a saturated CT closely related to third harmonic magnitude and angle in a HIF.

A comparison of these two waveforms in steady-state is shown in Figure 27. Although these two waveforms are not exactly equal, their similarity may affect the HIF algorithm which relies heavily on the magnitude and phase angle of the third harmonic. By inspection of the waveforms in Figure 27 shoulders can be noticed. What is not so evident from the waveforms is the phase-angle of the third or any other harmonic present in these waveforms. It is well understood that typical saturation of cores fixes the third-harmonic angle at  $\pm 180^\circ$ ; a similar angle is observed in a HIF.

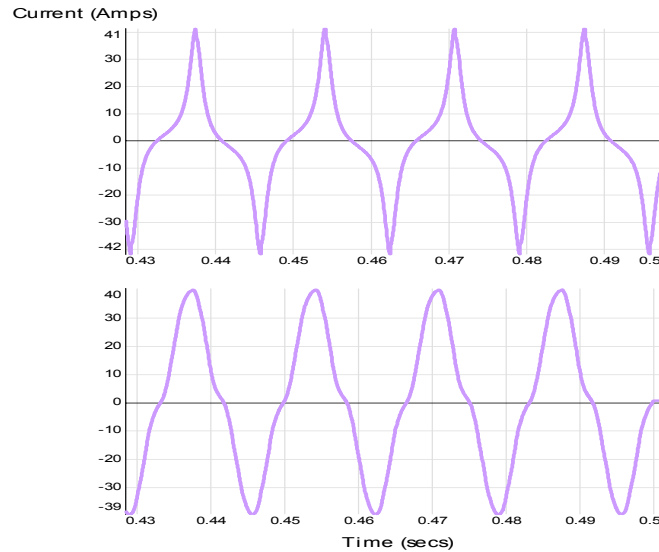


Figure 27. Comparison of a saturated CT waveform (top) and a HIF one (bottom)

For this study, an accurate and simple model for a saturable CT was not found readily available. Several methods and sources were investigated to model a variable-saturation core. It was found that the use of tables and data pairs normally solve the problem of modeling magnetizing branches, but it makes troublesome to model more than one type of saturable condition. The idea of creating an easy way (by means of an equation) to model a magnetizing branch or hysteresis curve was born. Following is detailed work of how this problem was approached.

#### **4.2. Impact of Saturated CTs in Distribution Feeders**

Saturation in ferromagnetic cores occurs when the flux's density reaches its maximum and the core starts showing the magnetic characteristic of free-space. The impact of saturated ferrites in electrical networks is of interest in protection, power quality, and other areas of study to avoid misinterpretations in current readings and to avoid harmonic injection or sinking in the system.

Several methods have been proposed to model the electrical behavior of a network in the presence of a saturated device during transients and in steady-state. Other works also model hysteresis loops with great precision but mainly to study inrush currents in transformers or accurate reclosure events [17] during transients. Other techniques exist where slopes and intercepts at various points of hysteresis loops are selected to calculate a model curve [18]. While also accurate, the need for many differential equations and ferromagnetic theory [17],[18] is not necessary when using the proposed methods of modeling hysteresis loops. Linearizing and magnetic circuits have also been implemented to model hysteresis loops by using straight-line approximations; an inconvenience is that linearizing only models the characteristics of one ferrite at a time and is not adjustable unless the data is re-tabulated. The study of HIF required a simple method for modeling hysteresis loops that did not use differential equations or ferromagnetic theory, but at the same time delivered an accurate model of the saturated condition.

The propose method of modeling a saturable CT not only shows an easy way to model hysteresis loops without using data pairs, but also shows that the magnetizing current of any hysteresis loops can be predicted/simulated by means of time-domain equation.

The aforementioned equations are not suitable for transient or inrush studies, but do avoid piecewise linearization. The philosophy of the flux equation is represented in Figure 28.

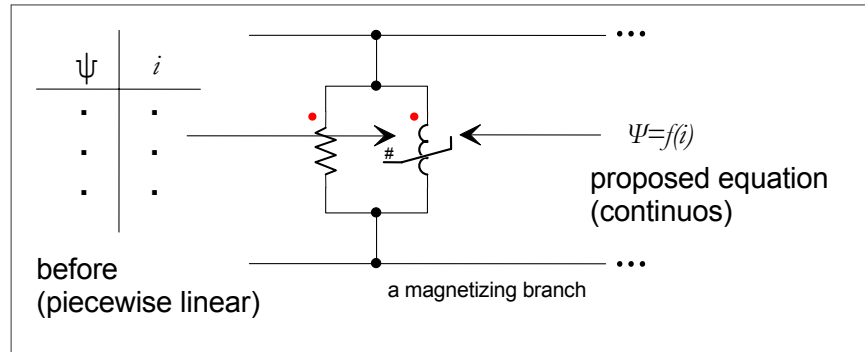


Figure 28. Modeling of a magnetizing branch to represent a saturable CT by means of an equation

### 4.3. Modeling CTs from Hysteresis Loops

The saturable characteristics of CTs, or any ferrite-based inductor, can be found from its saturation curves. A typical saturation curve is shown in Figure 29.

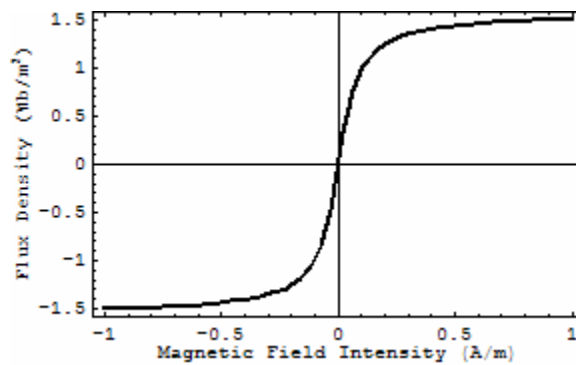


Figure 29. Typical saturation curve of ferrite

To model a hysteresis loop, a simple equation that approximates the flux as a function of the current is given by

$$\varphi(i) = \tan^{-1}(i) \quad \text{for } -1 < i < 1 \quad (1)$$

Equation (1) produced Figure 29. To avoid the slope of  $\varphi(i)$  from becoming too small or flat, the current is normalized and confined to  $\pm 1$ , otherwise, it will cause numerical instabilities as the same value of flux will appear to have multiple values of current. From (1), the units of  $\tan^{-1}(i)$  and therefore  $\varphi(i)$ , are in radians and limited to 1.57 as seen in Figure 29. This limitation is fixed by the introduction of a scalar  $M$  that adjusts  $\varphi(i)$  by scaling it; then the limiting 1.57 is no longer a constraint and the flux can be matched to experimental curves.

To control the slope of the flux in Figure 29, as it changes for different saturated conditions, the variable  $\rho$  is introduced. The variable  $\rho$  can be adjusted to match the slope of the flux as determined by a core's inductance. In experimental hysteresis curves, the slopes vary and are related to the effective relative-permeability  $\mu$ ;  $\rho$  accounts for this effect. Having introduced  $M$  and  $\rho$ , (1) becomes

$$\varphi(i) = M \tan^{-1}(\rho i) \quad (2)$$

When modeling hysteresis loops, an appropriate value for  $\rho$  in (2) must be chosen by inspection by comparing it to an experimental hysteresis loop. Figure 29 shows how (2) responds to changes in  $\rho$ .

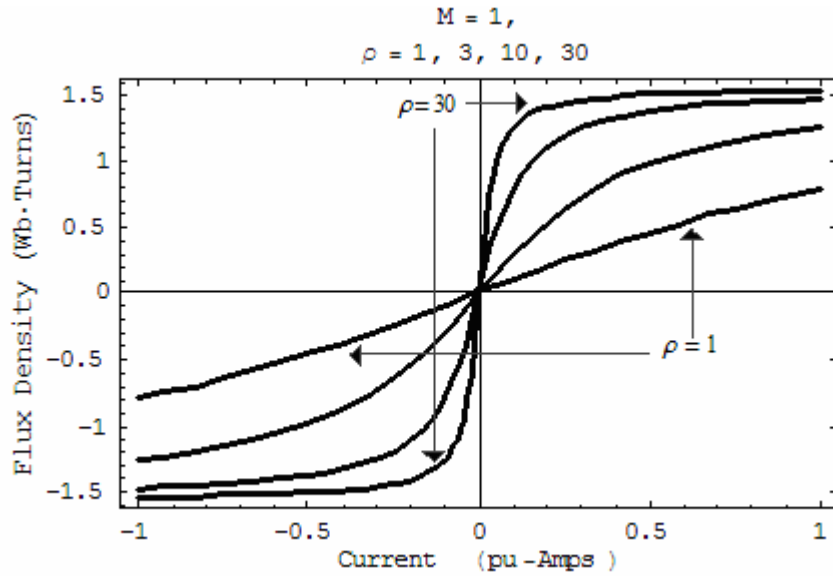


Figure 30. Flux curves using equation 2 for multiple values of slope  $\rho$

Figure 31 aids in choosing a correct value for  $\rho$  by inspection given an experimental hysteresis curve. So far, in determining the parameters of the flux equation, a value of  $\rho$  is chosen first by comparing it to the curves of Figure 29; then a value for  $M$  should be chosen to match the flux's peak. We see how plots of (2) in Figure 29 closely trace hysteresis curves in either incremental or decremental directions without linearizing. Equation (2) avoids the need for inputting a table of flux-current data pairs or piecewise linearization to model hysteresis loops as shown in Fig.1 or 3. Different saturable conditions can be modeled simply by changing the values of  $\rho$  and  $M$  in (2).

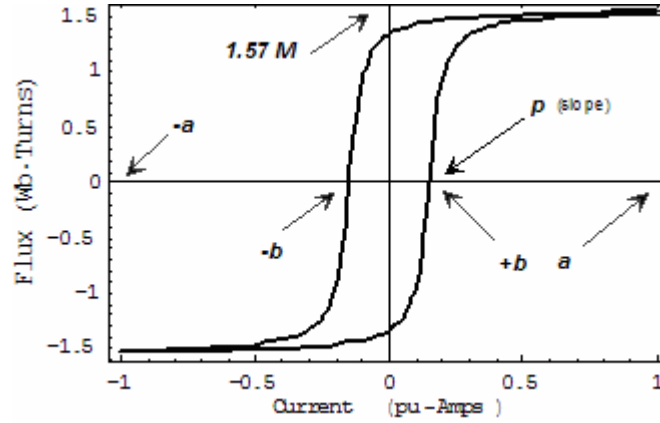


Figure 31. Hysteresis loop parameters

When a hard-core material is used, the gap of the hysteresis loop is more pronounced; therefore (2) must be modified to account for the double current-crossing presented by the hysteresis gap. Assuming no DC offset for the current, the flux will cross zero ( $\varphi=0$ ) in its incremental ( $\varphi_+$ ) and decremental directions ( $\varphi_-$ ) at exactly the same two magnitudes of current; at  $i=\pm b$  respectively as seen in Figure 29. Equation (2) is modified by offsetting the current by  $\mp b$  resulting in

$$\varphi(t) = M \tan^{-1}(\rho(i \mp b)) \quad (3)$$

From equation (3), the current is obtained as

$$i(t) = \frac{a}{\rho} \tan\left(\tan^{-1}(\rho) \sin(\omega t)\right) \quad (4)$$

where the flux  $\varphi(i)$  is represented as  $\varphi(t)=\sin(\omega t)$  since it remains sinusoidal inside the core despite the saturation. Using (2) and (4), multiple saturable conditions are modeled at ease. An example showing various scenarios is shown in Figure 29.

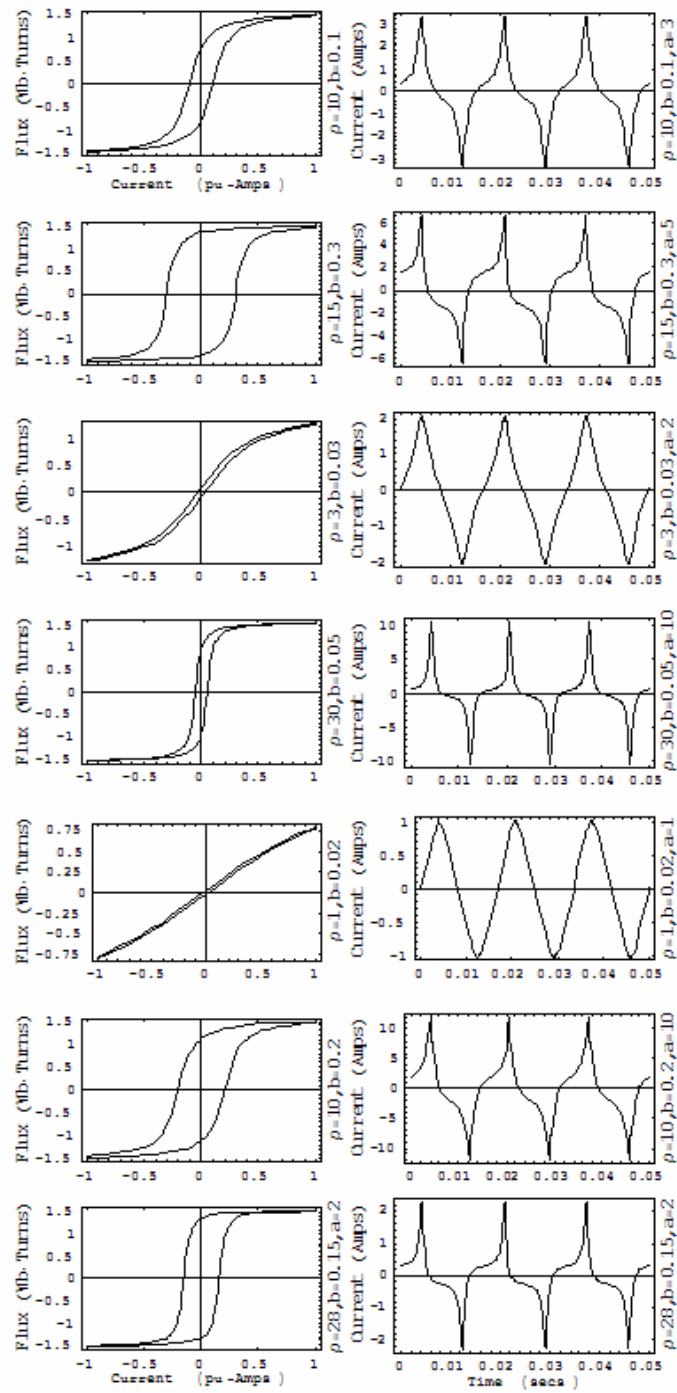


Figure 32. Multiple saturable conditions showing hysteresis loops and their magnetizing currents based on equations 2 and 4

Detailed information on hysteresis loop and magnetizing current modeling can be found in [16], where details of the CT model are better explained.

In Simplorer®, the saturable CT can be represented by a current source driven by (4). When saturated, it forces the higher amplitude current waveform of Figure 29.

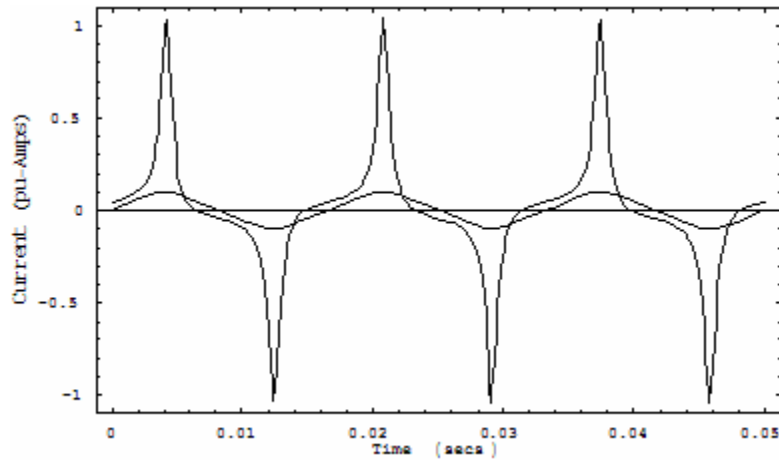


Figure 33. CT linear and saturated currents in steady-state (pu-Amps)

The harmonic content of Figure 33 for the saturated case, was extracted in Simplorer® by using the test circuit shown in Figure 34

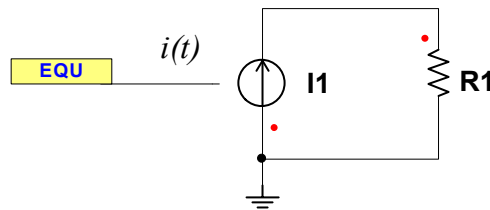


Figure 34. Sample circuit to extract Fourier spectrum for saturable CT

The equation block in Simplorer® can be filled with the  $i(t)$  equation and then fed as the current source driver. This ability of forcing the current source to an external equation is

another feature of Simplorer® that made it the software of choice. The spectrum of the saturated current is shown in Figure 35.

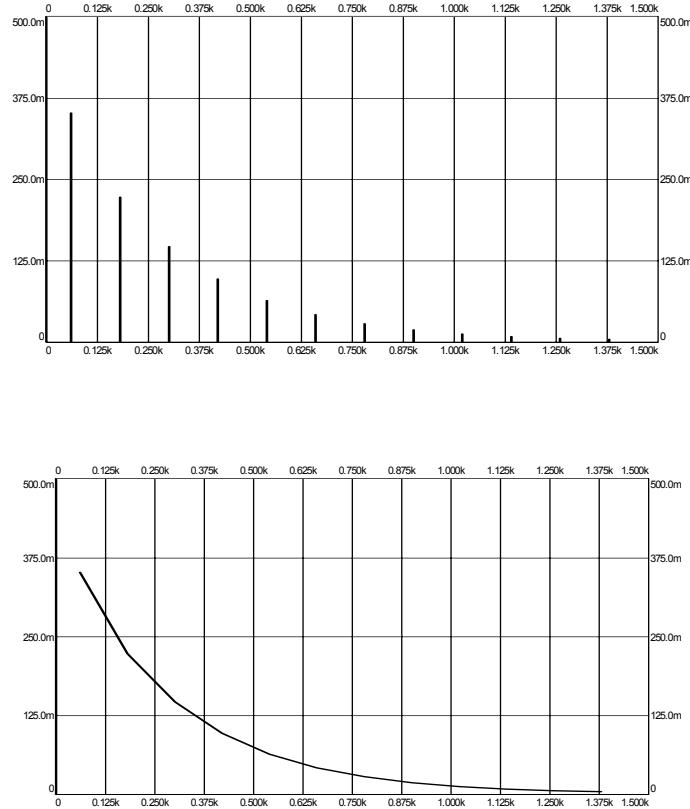


Figure 35. Current spectra of saturated CT current.  
(top: actual spectrum. bottom:  $1/f$  analog relationship)

As expected, the Fourier spectrum of a saturated CT shows only odd-order harmonics following a  $1/f$  pattern. This is a characteristic of ferrite saturation and agrees with a real-life condition. No even harmonics are present because the wave is symmetric and periodical. It can be seen that the 3<sup>rd</sup> harmonic current is the dominating non-fundamental component and may lead to false HIF triggers. The proposed algorithm to detect HIFs will account for this condition.

#### 4.4. Comparison between CT and HIF Curves

The hysteresis loop modeled by the CT can be compared to the one of a HIF presented by KEPCO's model. These two are shown in Figure 36.

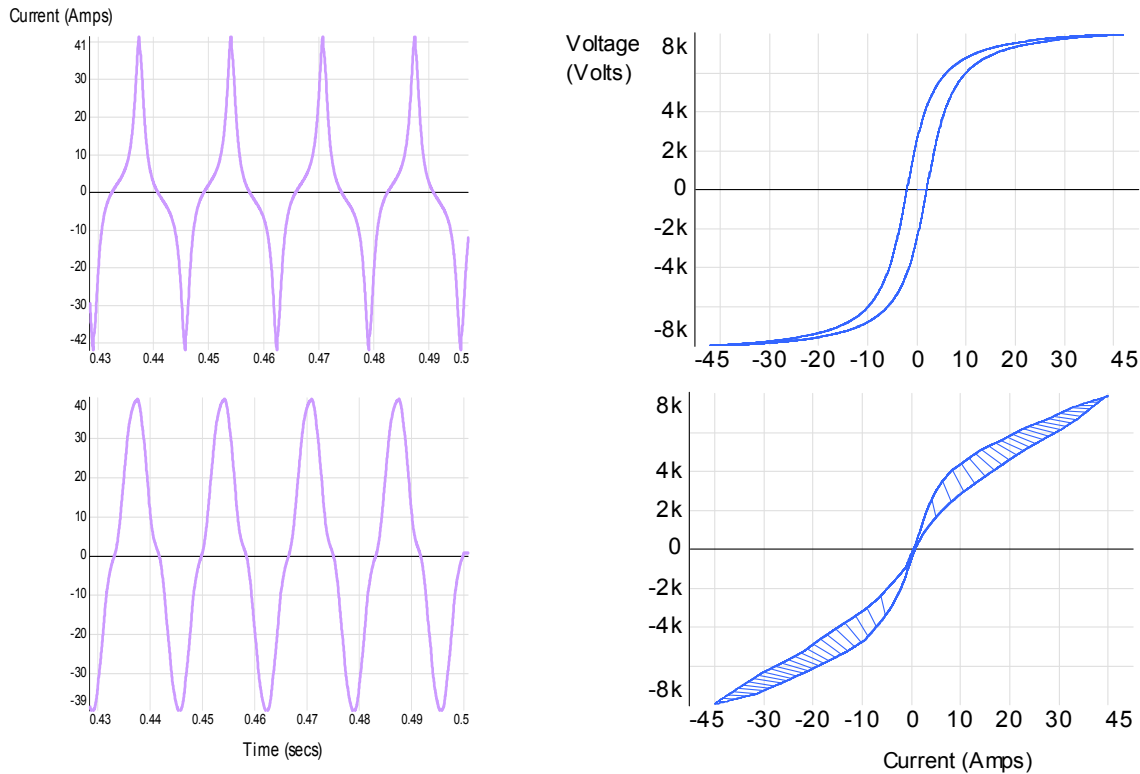


Figure 36. Comparison of hysteresis loops of a CT (top) and a HIF (bottom)

It can be seen from that the HIF presents highly non-linear impedance (slope of V-I characteristic). The CT hysteresis loop also shows that the CT model developed is accurate; it presents a “nearly perfect” hysteresis loop. The comparison of these two curves, and the ability of obtaining real-time (in-progress) magnitude and phase information in Simplorer® allows for testing the algorithm for discrimination between a HIF and a saturate core.

## Chapter 5: Algorithm Criteria and Discussion

### 5.1. Using the Third-Harmonic Current-Angle

As has been shown in past work of other researchers and institutions [12],[13],[14] and summarized in Table 2, the third harmonic-current angle is a strong representative or indicative of the presence of a HIF. It is not the only indicative, but certainly a strong one and it can be accurately measured for phase changes. At a common sampling rate of, say,  $f_s=10$ -kHz or  $T_s=0.1$ -ms we can sample the third harmonic at every  $6.5^\circ$  during its  $360^\circ$  revolution. Summarized below is a table of how often we can extract a rotating harmonic based on a sampling frequency and harmonic number.

A sampling frequency of: →	...for the n <sup>th</sup> harmonic: →	...having a cycle of: →	...would be measured every: $\frac{360 n f_0}{f_s}$
1 kHz / 1 ms	3 <sup>rd</sup> 5 <sup>th</sup> 7 <sup>th</sup> 15 <sup>th</sup>	180 Hz / 5.55 ms 300 Hz / 3.33 ms 420 Hz / 2.38 ms 900 Hz / 1.11 ms	64.86 degs 108 degs 151 degs 324 degs
8 kHz / 125 $\mu$ s	3 <sup>rd</sup> 5 <sup>th</sup> 7 <sup>th</sup> 15 <sup>th</sup>	180 Hz / 5.55 ms 300 Hz / 3.33 ms 420 Hz / 2.38 ms 900 Hz / 1.11 ms	8.1 degs 13.5 degs 18.9 degs 40.5 degs
10 kHz / 0.1 $\mu$ s	3 <sup>rd</sup> 5 <sup>th</sup> 7 <sup>th</sup> 15 <sup>th</sup>	180 Hz / 5.55 ms 300 Hz / 3.33 ms 420 Hz / 2.38 ms 900 Hz / 1.11 ms	6.48 degs 10.8 degs 15.12 degs 32.4 degs
50 kHz / 0.02 $\mu$ s	3 <sup>rd</sup> 5 <sup>th</sup> 7 <sup>th</sup> 15 <sup>th</sup>	180 Hz / 5.55 ms 300 Hz / 3.33 ms 420 Hz / 2.38 ms 900 Hz / 1.11 ms	1.29 degs 2.16 degs 3.02 degs 6.48 degs

Table 10. Follow-through table showing how accurate a phasor can be measured

It can be noticed from Table 10 that the higher  $f_s$ , the more often and therefore more accurate the third harmonic phasor can be measured. The recloser and sectionalizer assumed for this implementation have a sampling rate  $f_s=8$ kHz, so Simplorer® was set also to this value in the FFT block. Again, Simplorer® can sample at any specified value but it is set at 8-kHz to

simulate real-life equipment. The distribution feeder model and the disturbance points are illustrated below

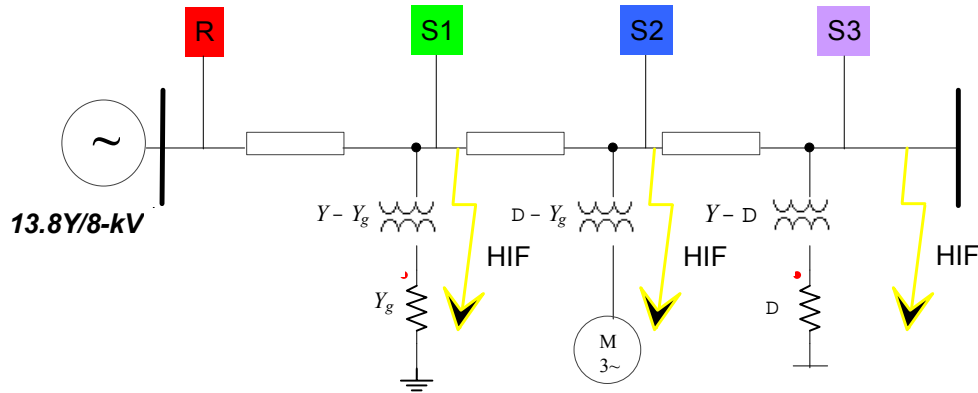


Figure 37. Distribution feeder showing HIF disturbance points

The harmonic content seen from the recloser R and sectionalizers S1, S2, and S3 will be shown. Communication is assumed to be available between these devices and therefore they can compare spectral content among each other and determine where the HIF is located. From the literature review, it is gathered that the angle position of the third harmonic current  $\varphi_3$  reveals a certain characteristic about the HIFs. As the HIF current builds-up, as shown in Figure 22 so will the difference between  $\varphi_3$  and the fundamental voltage.

A flow chart showing with the criteria assumed by each sectionalizer is shown next. Any sectionalizer, say  $k$ , must declare an HIF before comparing its result with sectionalizer  $k+1$ . Since the distribution system is radial, protection is assumed directional. Hence, sectionalizers  $S_k, S_{k+1}, S_{k+2}, \dots, S_{k+n-1}$  all look for “in-front” faults and not for “behind” ones.

Before  $S_k$  can start looking for HIFs, it must build-up memory; that is, it needs to know (store) the ambient current and voltage on the line. It does this by taking at least four samples, from  $i=0$  to  $i=4$  where the  $i^{\text{th}}$  measurement  $M_i$  is stored every time. After four samples ( $i>4$ ), the fifth measurement  $M_5$  will be compared to the measurement taken four samples ago  $M_1$ . If there exists a load step (not a load dump) within the range  $0.05p\mu < \Delta M < 0.8p\mu$  where these limits can be adjusted at anytime, the first flag will be set to =1. Following this flag, the



algorithm checks for a similar condition in the other two phases to confirm a single phase HIF. Since the HIFs assumed in this work are single phase, bi- or three-phase faults are not considered. For single-phase faults, the sectionalizer will start to extract the harmonic content of the line current. If the angles of 3<sup>rd</sup> and 5<sup>th</sup> harmonics settle to within the ranges specified following a progressive build-up the persistence of the fault for 0.5 seconds will be checked. If the fault still exists after 0.5 seconds, it will be compared against the total increment in line current that must be within 0-100A as is typical for HIFs. Table 1 is copied below for convenience.

MATERIAL	CURRENT (AMPS)
Dry asphalt	0
Concrete (non-reinforced)	0
Dry sand	0
Wet sand	15
Dry sod	20
Dry grass	25
Wet sod	40
Wet grass	50
Concrete reinforced	75

Table 11. Typical HIF current values for <15kV distribution feeders

All sectionalizers  $S_k$  through  $S_{k+(n-1)}$  are processing the information described above and shown on the flow chart simultaneously. If  $S_k$  declares the presence of a HIF on the line, its result will immediately be compared to  $S_{k+1}$  's. Should they disagree on the reading (i.e.  $S_k=1$ ,  $S_{k+1}=0$ ), then the fault must lie in between these two sectionalizers. If they agree on the reading ( $S_k=1$ ,  $S_{k+1}=1$ ), then  $S_{k+1}$  will compare its results with  $S_{k+2}$ . The comparison process will continue indefinitely until  $S_{k+x}$  's result disagrees with  $S_{k+x+1}$  's result. A simple C++ code for an outer algorithm that is constantly checking the values of the sectionalizers is shown below.

```

n=...;                /*number of sectionalizers in the line*/
for k=1:n:n++        /*initializes flags to 0*/
{
    S[k]=0;          /*array of sectionalizers*/
}
k=1;
DO WHILE (S[k]==S[k+1]) /*compares inter-sectionalizer results*/
{
    k++;
}
printf('HIF present between S[' ,k,'] and S[' ,k+1,']');
cin << ('Trip recloser? (y/n) ');    /*user intervention required*/

```

This code will declare a HIF and prompt attention from the control house engineer. Depending on the location and type of fault, the operator's decision will terminate the fault.

## Chapter 6: Simulation Results

For each simulation, power flow is conducted to determine the steady-state power demand of all the loads. This is necessary to ensure that the modeled loads actually reflect a real-life scenario and that no unusual circumstances have been created by mistake. A phasor diagram showing the VA requirements in steady-state is shown below.

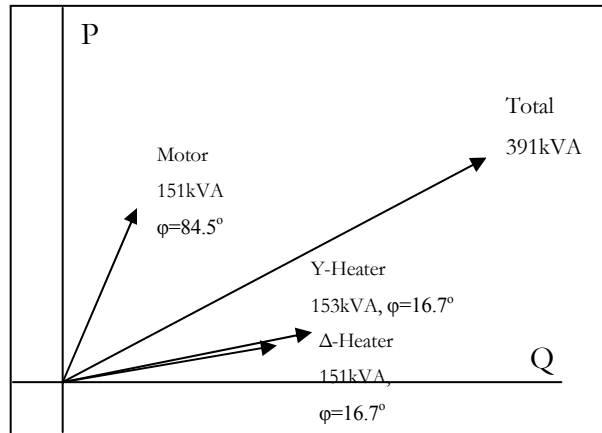


Figure 39. Loading power demand phasors

The motor shows an inductive behavior; this was expected. The heaters present a small power factor angle due to the reactance in the transformer before them. The power measurements are made as seen by the feeder and not as consumed by the end-load.

### 6.1. A Foreword on the Results

The results shown in this section are based on what the sectionalizers measure in the line current. It is assumed that the feeder has reached steady-state and that no transients are in progress. Also, that the generation frequency is fixed at 60-Hz. A variation in these conditions would have an impact on the sectionalizer readings. The principal criteria for detecting a HIF are the angles of the third and fifth harmonics which are only computed if their magnitude is greater than the minimum specified of 1-pu as seen from the flow chart in

Figure 38. To ease the interpretation of the simulation results, the harmonics are given colors following the standard and well-known resistor color-scheme. These are shown in Figure 40.



Figure 40. Harmonic color-coding based on standard resistor colors

The HIF model implement is placed on different sections of the line to test the designed algorithm. In addition, the algorithm is tested for discrimination against a saturated CT which may create confusion for the sectionalizers. Each time a HIF is simulated, the readings of all sectionalizers are shown graphically. This enables visual comparison and validation of the proposed algorithm.

## 6.2. Fault after First Sectionalizer

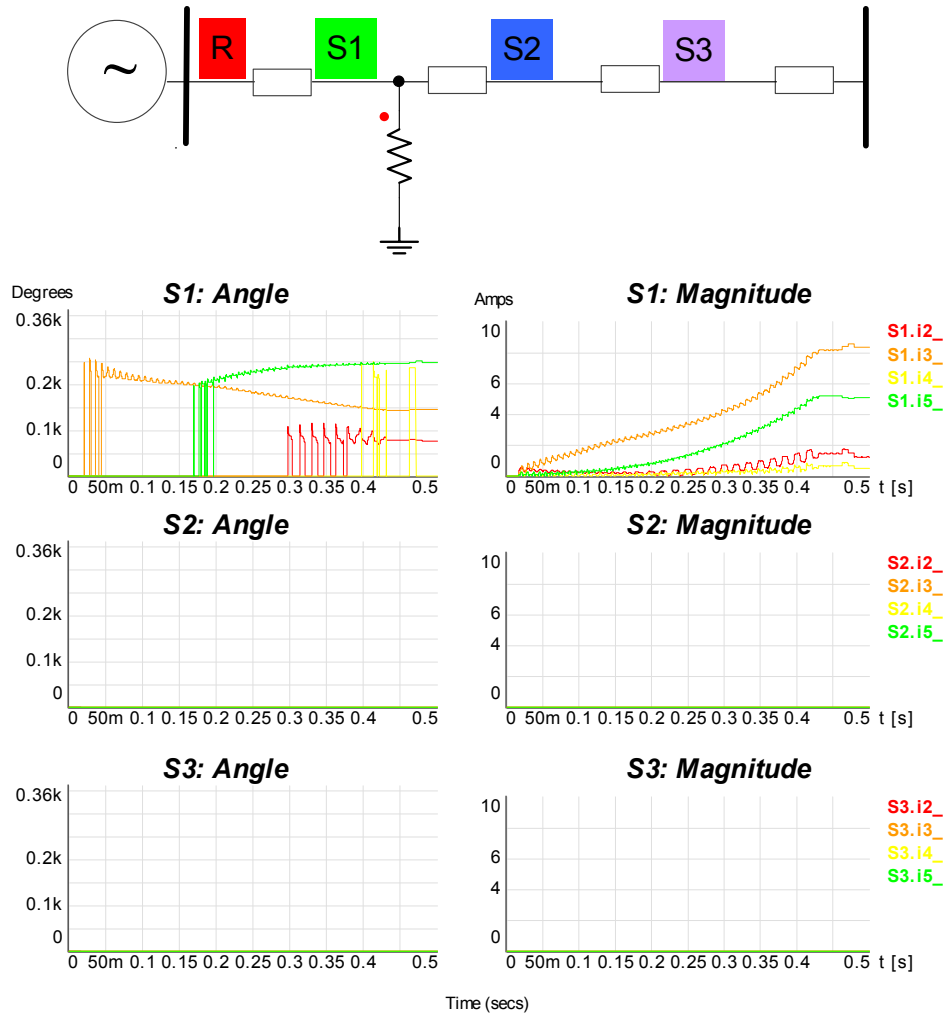


Figure 41. Fault after S1

For a fault in front of sectionalizer one ( $S_1$ ), only  $S_1$  sees the fault. From the magnitude plots, it can be seen that the first five harmonics exist in the HIF. The existence of the 2<sup>nd</sup> and 4<sup>th</sup> harmonics is due to asymmetry in the HIF waveform. This is not a decision flag, but it is noted that they are present and that the 2<sup>nd</sup> harmonic remains at  $\sim 77^\circ$ . To reduce the computational burden on the recloser and sectionalizers during the build-up period, the algorithm will not compute angles for harmonics whose magnitude is less than 1A.

Sectionalizers 2 and 3 ( $S_2$  and  $S_3$ ) don't see the fault because the harmonic content 'exits' the feeder through the HIF branch leaving the remaining of the line undisturbed.

The 3<sup>rd</sup> and 5<sup>th</sup> harmonic angles have opposite yet similar behaviors. The 3<sup>rd</sup> harmonic shows a constant 'decrement' during the build-up period until it settles at  $\sim 145^\circ$ . Similarly, the 5<sup>th</sup> harmonic shows a constant 'increment' during build-up until it settles at  $\sim 245^\circ$ . Their transient regimes are limited to the build-up period only. Once the HIF reaches steady-state ( $\sim 0.5$  secs.) they will maintain a fixed angle. The build-up period might vary from HIF to HIF, so this condition by itself is not enough for detection.

From the magnitude information, it can be determined that the odd-harmonic spectrum (3<sup>rd</sup>, 5<sup>th</sup> ...) will follow a  $1/f$  relationship just as it did for the CT (Figure 36). This is another reason why the HIFs are compared to the CT's behavior in steady-state. From the angle measurement plots in Figure 41 it can be noted that the angles fluctuate from a certain reading to zero and back, like a pulsating (square) wave. This is due to their respective magnitudes becoming less than 1A at times thus stopping the calculation of the harmonic angles (must be  $>1A$  to measure).

From the magnitude observations, it can be determined that the odd-harmonic spectrum (3<sup>rd</sup>, 5<sup>th</sup> ...) will follow a  $1/f$  relationship just as it did for the CT (Figure 36). This is another reason why the HIFs are compared to the CT's behavior in steady-state. From the angle measurement it is noted that the angles fluctuate from a certain reading to zero and back, like a pulsing wave. This is because their respective magnitude becomes less than 1A at times making the angle measurement disappear.

### 6.3. Fault after Second Sectionalizer

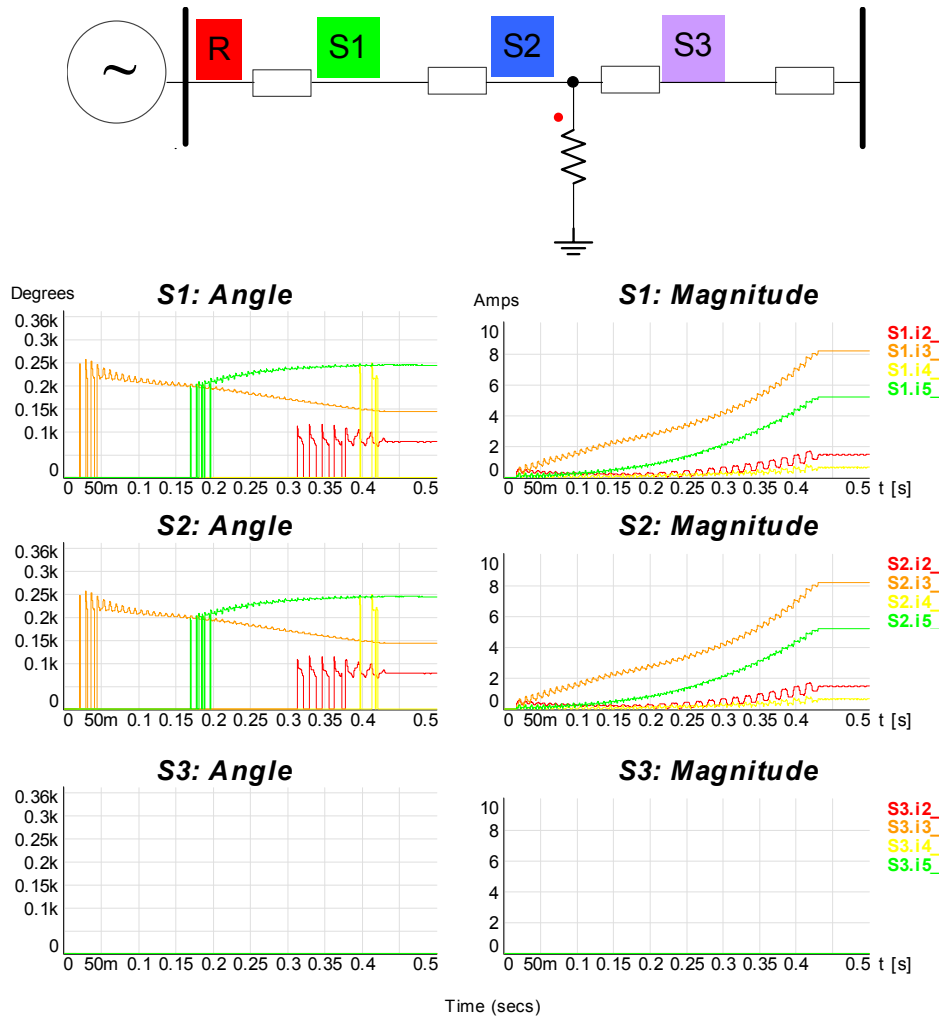


Figure 42. Fault after S2

For this case both  $S_1$  and  $S_2$  see the fault, but not  $S_3$ . These results indicate that the harmonic content will not travel beyond the HIF point. It can be concluded that the fault always lies between the last sectionalizer that acknowledges the fault and the first sectionalizer that doesn't. We assume that communication between sectionalizers is fast, effective, and accurate, so their comparison as to what they see becomes the basis of localization. This result is verified in the next test.

## 6.4. Fault after Third Sectionalizer

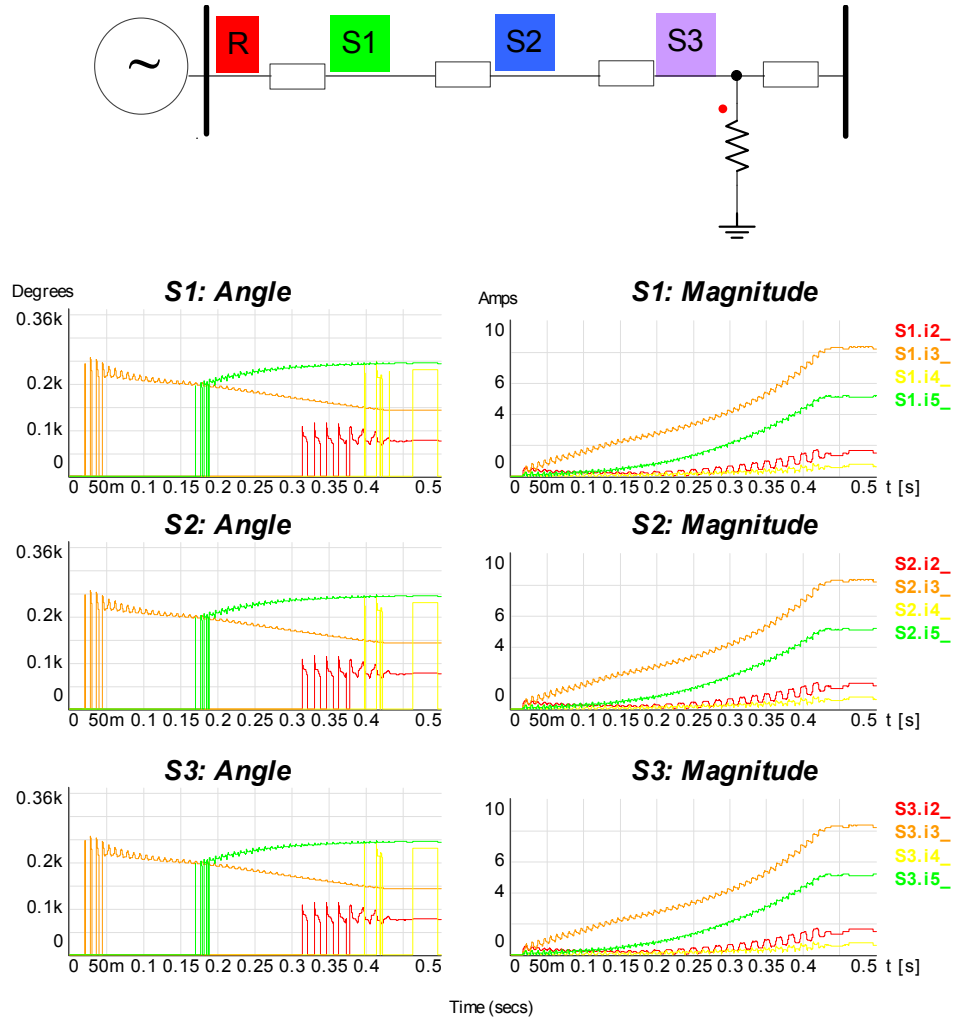
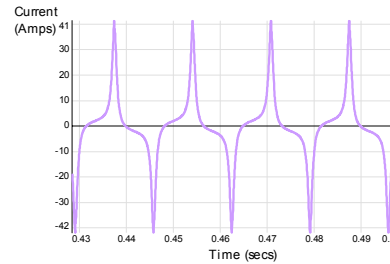
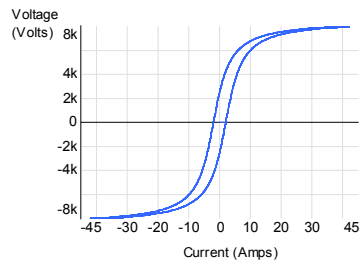
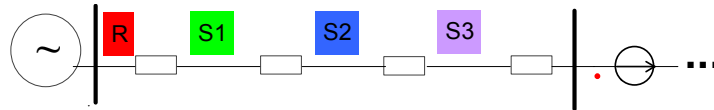


Figure 43. Fault after S3

All sectionalizers now see the same fault content and determine that the fault is present downstream of  $S_3$ . The last sectionalizer to see the fault is always the one in most proximity to the fault. This sectionalizer (the closest to the HIF) sends the alter signal reporting the fault.

## 6.5. Distinguishing HIFs from CTs

The potential problem that CTs present at various saturation levels is the similarities in harmonic phase-angles. From the model developed in Chapter 5, multiple saturation levels are tested for harmonic-angle similarities and differences. The following diagrams show the per-phase test situation, hysteresis saturation level, and time-domain current.



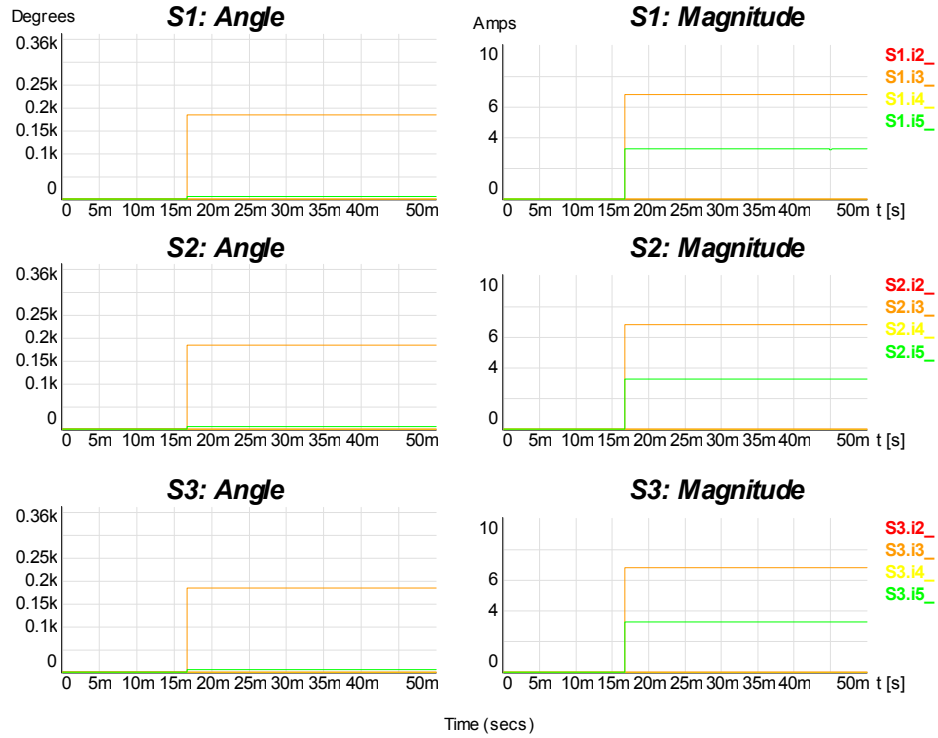
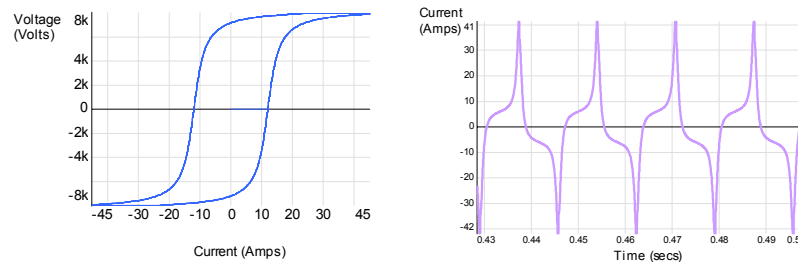


Figure 44. Sectionalizer readings for a saturated CT

for saturation level  $\rho=30$ ,  $b=0.05$ ,  $a=40$

Only the incremental current of the CT's primary was captured ( $\sim 40A$ ). It is known that the CT sees 200-600A during normal operation. During steady-state, the angle measurements did not see a 5<sup>th</sup> harmonic angle despite its magnitude existence above 1A. This indicates that for a CT, the 5<sup>th</sup> harmonic angle remains at 0° whereas for the HIF it is 244°. This important result allows us to use the 5<sup>th</sup> harmonic as a discriminatory flag against saturated ferrites in the detection of HIFs.



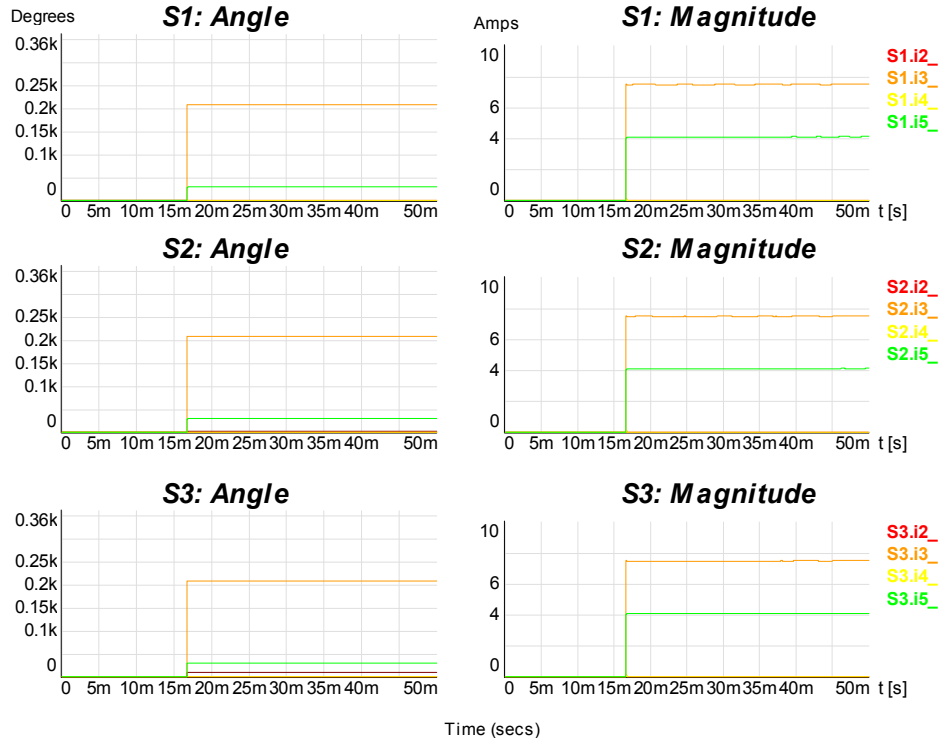
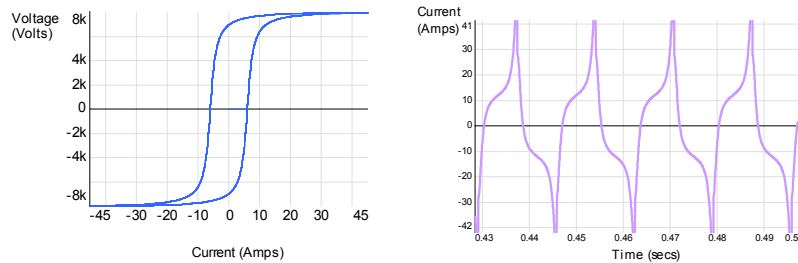


Figure 45. Sectionalizer readings for a saturated CT

for saturation level  $\rho=15$ ,  $b=0.3$ ,  $a=40$

For this test, the CT presents a harder core. The hysteresis gap (or energy required to invert magnetic dipoles) is larger as seen from Figure 45. This kind of core has a direct effect on the 5<sup>th</sup> harmonic angle which now has risen to 30°. The change of core (or saturation level) had a 1A effect on the magnitude. Since magnitude is not a decision criterion, we pay more close attention to the angle. Another CT saturation level is tested to insure that the 5<sup>th</sup> harmonic angle remains below than the 3<sup>rd</sup> as has been in shown in Figure 45 and Figure 45.



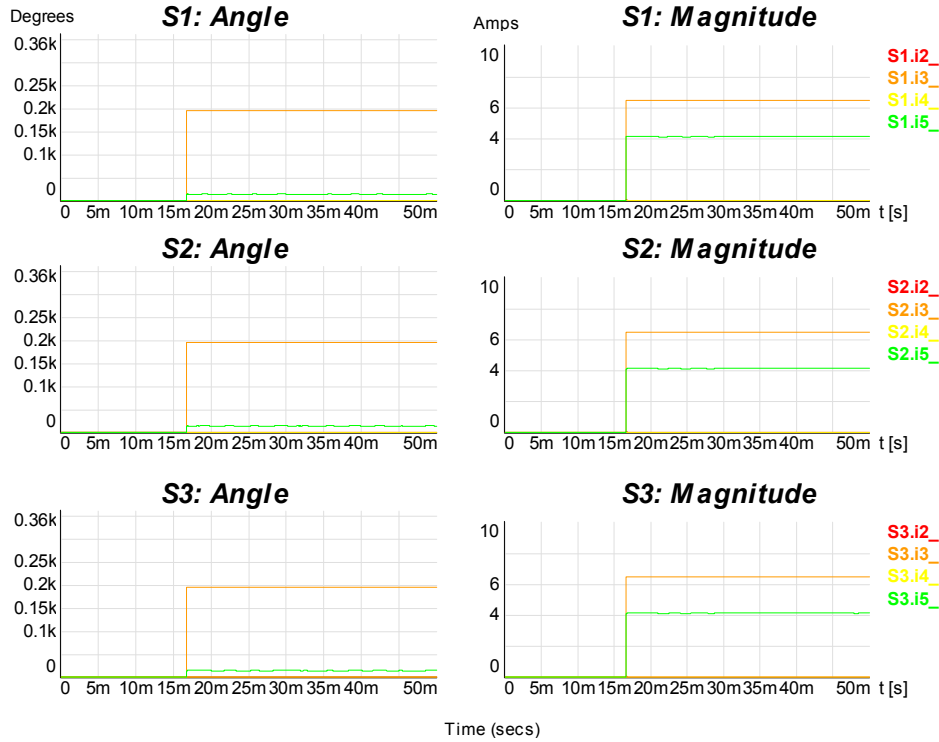


Figure 46. Sectionalizer readings for a saturated CT

for saturation level  $\rho = 28$ ,  $b = 0.15$ ,  $a = 40$

This hysteresis loop represents a semi-hard core with high saturation at its operating point. From the sectionalizer readings, the 5<sup>th</sup> angle barely exists at 14°. The above three CT saturation cases all gave a 5<sup>th</sup> harmonic angle of less than 30°. It can be determined that a high 5<sup>th</sup> harmonic angle ( $\sim 245^\circ$ ) as shown in Figure 41 is proprietary of a HIF. This is the criteria that will distinguish between a HIF and a temporary saturated CT.

## 6.6. Testing Under Motor Loading

Other transient conditions such as motor load-stepping affect all three-phases, but may be sustained (duration  $>0.5$  secs) thus triggering one of the algorithm flags. When such conditions occur, the third harmonic doesn't generally exist at all; but when it does, it only exists during a very steep increment of load (when  $di/dt$  is very large). After this, it disappears immediately. Also, if  $di/dt$  is large and sustained, it will very likely exceed the 0-100A typical HIF current limits shown in the flow chart algorithm and will not set the flags. Following are graphical results of what happened when the induction motor was given an abrupt load-step of 1000-Nm from running an synchronous speed and being unload.

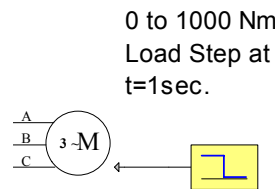


Figure 47. Schematic representation of HIF algorithm being tested against abrupt motor loading

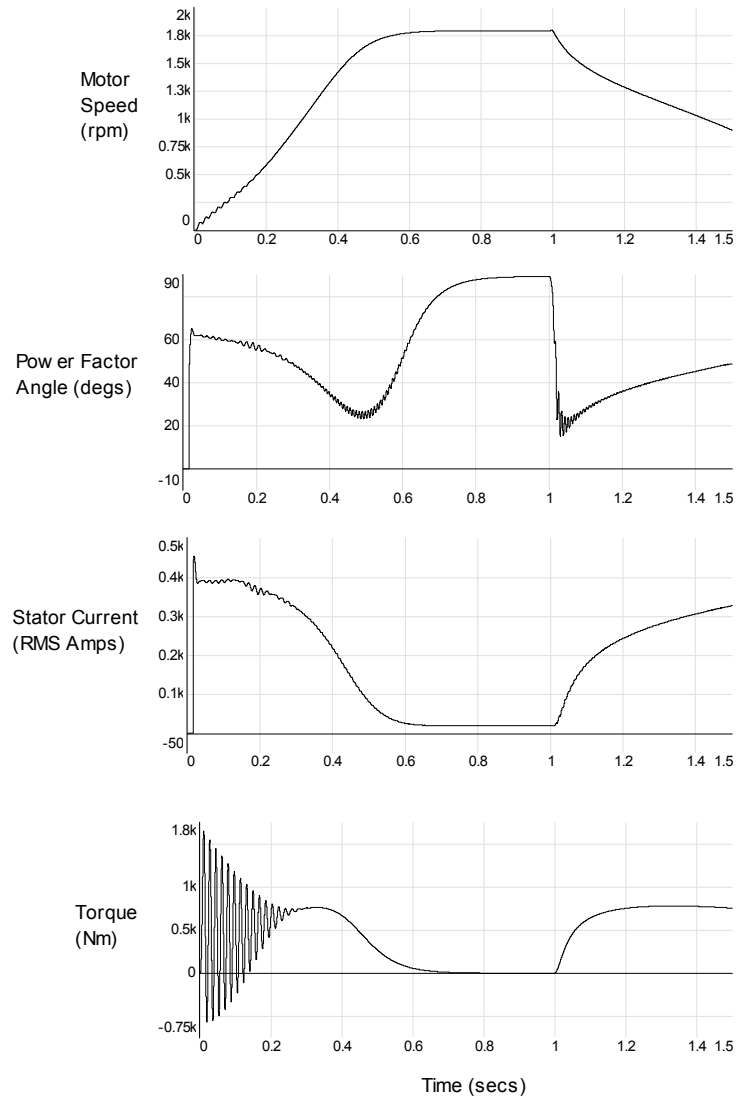


Figure 48. Motor response under abrupt loading at  $t=1s$

When the motor is loaded abruptly as shown in Figure 48, the stator current's  $di/dt$  response is not so pronounced due to the moment of inertia (see Appendix B) of the motor. This results in the non-existence of the third-harmonic current during this transient.

## 6.7. Testing Under HIFs with Shoulder

High-impedance faults that present a shoulder during build-up are rare. If they do occur, the proposed algorithm will still detect them because they have the same form of steady-state current. Also, the duration would be even larger than the known  $\sim 0.4$  seconds due to the shoulder effect, so the duration flag will be set. The third and fifth harmonic angles also stabilize at  $\sim 180^\circ$  and at  $\sim 220$  respectively in the steady-state regime; so there is no difference in angles as seen by the sectionalizers. The only difference is the duration of build-up. These results are shown graphically as seen from any sectionalizer  $S_k$  before the fault

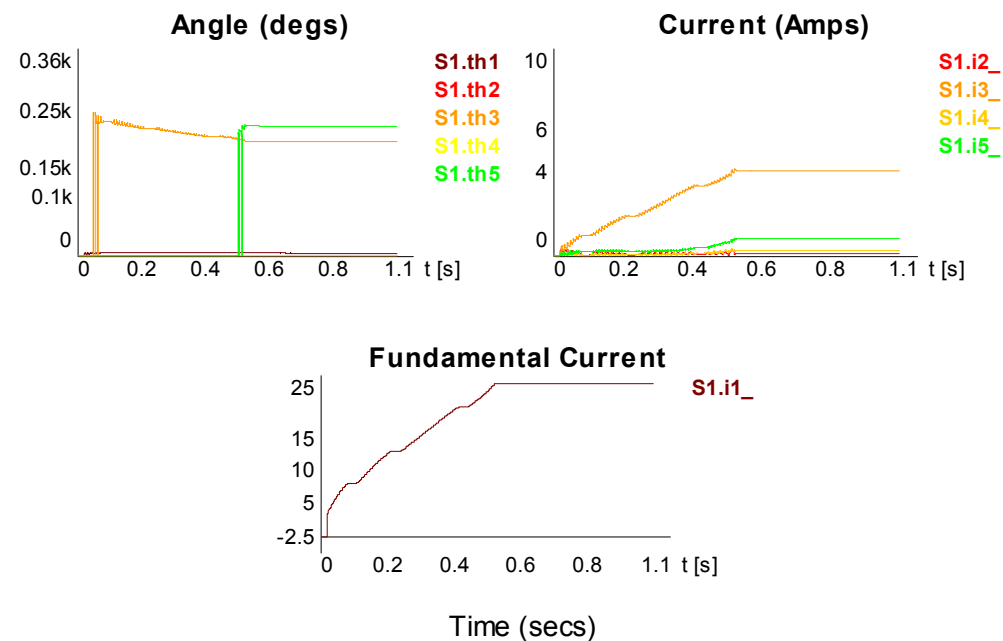


Figure 49. Shoulder-present HIF harmonic-phase analysis

The fundamental current in Figure 49 shows a shoulder during the build-up period. This occurs in some HIFs, but not all. The HIF algorithm proposed will also detect such conditions.

## Chapter 7: Final Gatherings

### 7.1. Summary

A 13.8-kV, 4-wire, radial distribution feeder of about ~20 miles in length is put together in Simplorer®, a powerful and complete circuit simulation software. The feeder's line losses are computed based on what is typical for line current such that the far-end voltage is within  $\pm 5\%$  of nominal conditions. The loads fed by the system were chosen and modeled carefully one at a time to insure realism. Beginning with phase step-down transformers, their leakage impedances were chosen from typical values found in power systems textbooks[2],[5]. Then, appropriate loads were chosen for the feeder to simulate real-life conditions; among them, purely resistive loads, and an induction motor. Fictitious loading was modeled in the form current sources that delivered current downstream of the feeder's far-end. They sank ~500A and made the system more realistic.

High-impedance faults are not detectable by conventional protection schemes, so an algorithm is developed that performs harmonic-angle analysis to declare these faulted condition. The algorithms are to be programmed/loaded in sectionalizers that have the ability of comparing their results with the next sectionalizer downstream. Communication among sectionalizers is assumed dependable and secure. Should two adjacent sectionalizers ( $S_k$  and  $S_{k+1}$ ) disagree on the presence of a faulted condition, the algorithm will declare the presence of a HIF in between  $S_k$  and  $S_{k+1}$  and will alert it to the control house.

Saturated CTs have the problem of showing similar current characteristics of an HIF. A saturated can confuse the HIF detection algorithm and make it think that a HIF is present when its really not. This problem arises from the strong dependence of the proposed algorithm to the position of the 3<sup>rd</sup> harmonic current angle. Both HIFs and saturated CTs fix the third harmonic angle within the 150-250° range. Other flags must then be checked for to distinguish from these two conditions. These two conditions are tested and analyzed and differences are found due to the presence of the angle of the 5<sup>th</sup> harmonic during a HIF, and not during CT saturation.

## **7.2. Conclusions**

Most high-impedance faults can be detected using harmonic-current phase-angle analysis and localized by using recloser-sectionalizer technology. In microprocessor-based detectors such as sectionalizers, various typical HIF patterns must be programmed to the module in the form of detection flags. Sectionalizers will constantly be looking for these typical patterns of a HIF as provided in this work. If the current patterns meet the detection criteria, adjusted sectionalizers will communicate with each other in trying to locate the fault.

The presented work assumes single-phase faults since they account for the greater majority of HIFs. Due to the strong harmonic-angle dependence, transient conditions in distribution feeders can cause false readings. These are overseen by the detection algorithm that discriminates against multi-phase and short-duration effects. For instance, capacitor switching would be of very short-duration (1-3cycles) and would happen in all three-phases. High-impedance faults are normally single-phase and are sustained.

## **7.3. Future Work**

When CTs saturate, there is no way to know for sure what the primary current is. This means that the measurements taken by protection equipment are incorrect. It is said that the current in the CT's burden is unusable or *garbage* because it does not represent accurately what is happening in feeder's line. From the given hysteresis loop modeling equations of Chapter 4, the primary current can be predicted knowing the equations for the saturation curves. The flux equation can closely trace the saturation curve of any homogeneous saturable core. If this equation is further analyzed and studied, the primary current can be predicted when the CT enters the saturation region. An equation for the primary was derived as  $i(t)$ , but it is assumed that the amplitude  $a$  was known. In a saturated CT, the primary's amplitude  $a$  is never known.

Models for bi- and three-phase HIFs are not readily available. Most HIF models exist for single-phase to ground faults. The creation of electrical models for these HIFs would help research and further development of algorithm for HIF detection. It must be considered that the microprocessors will need constant updating each time a new HIF detection algorithm is proven accurate. As new HIF models become available, algorithms can be created to detect these and fed into the microprocessors.

## Appendix A: Measuring three-phase power

Simplorer® does have a part to measure three-phase power directly, but a method referred to as the *two-wattmeter method* can be used. Placing two wattmeters that read instantaneous power, as shown in Fig.A1, and extracting its mean (average) suffices to find  $P$ ,  $Q$ ,  $S$ , the power factor (PF), and the power factor angle  $\varphi$ .

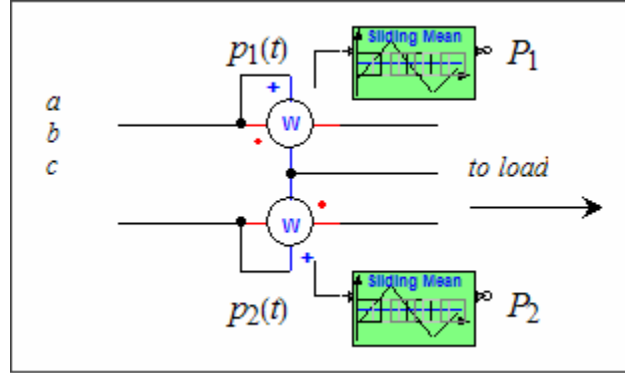


Fig. A.1. Two-wattmeter connection schematic

The wattmeters read instantaneous power  $p(t) = v(t)i(t)$ , and not RMS power as desired. By definition RMS power is also the average power; therefore  $p(t)$ , as read by the wattmeters, can be averaged to obtain the RMS quantity wanted. From Fig.A1,  $p_1(t) = v_{ab}(t)i_a(t)$ , then the RMS power is

$$P_1 = \frac{1}{T_0} \int_t^{t+T_0} p_1(t) dt = V_{LL} I_L \cos(\varphi + 30^\circ)$$

In the same manner,  $P_2$  is given by

$$P_2 = \frac{1}{T_0} \int_t^{t+T_0} p_2(t) dt = V_{LL} I_L \cos(30^\circ - \varphi)$$

where an error of  $\pm 30^\circ$  for  $P_1$  and  $P_2$  respectively is introduced because of the line-to-line measurements and not line-to-neutral ones. The relationship between the line-to-line ( $V_{LL}$ ) and line-to-neutral voltages ( $V_p$ ) are  $V_{LL} = \sqrt{3}V_p e^{j30^\circ}$ . The (total) three-phase RMS power  $P_3$  is found by adding  $P_1$  and  $P_2$  as

$$\begin{aligned} P_3 &= P_1 + P_2 \\ &= V_{LL} I_L (\cos(\varphi + 30^\circ) + \cos(-\varphi + 30^\circ)) \\ &= \sqrt{3} V_{LL} I_L \cos(\varphi) \end{aligned}$$

From similar mathematical derivations [5], it can be shown that the three-phase reactive power is extracted from the difference

$$\begin{aligned}\frac{Q_3}{\sqrt{3}} &= P_2 - P_1 \\ &= V_{LL} I_L \sin(\varphi) \\ \Rightarrow Q_3 &= \sqrt{3}(P_2 - P_1)\end{aligned}$$

Only  $P_3$  and  $Q_3$  are needed to find  $S_3$ ,  $PF$ , and the power factor angle  $\varphi$  as

$$\boxed{\begin{aligned}S_3 &= \sqrt{P_3^2 + Q_3^2} \\ PF &= \frac{P_3}{S_3} \\ \varphi &= \tan^{-1}\left(\frac{Q_3}{P_3}\right)\end{aligned}}$$

## Appendix B: Moment of inertia of a machine

All machines have rotors with certain mass and cross-sectional area. These two parameters determine the moment of inertia  $J$  of the machine in the units of  $kg\cdot m^2$  or  $N\cdot m\cdot s^2$ . Both units are equivalent in the SI, but Simplorer® requires the value in  $kg\cdot m^2$ . The moment of inertia is a particular property of the machine that tells us how much initial torque must be applied to its rotor to begin rotation. It accounts for the weight of the shaft and not for frictional or damping losses.

The linear kinetic energy of a particle is given by  $W=1/2mv^2$  but it does not apply for rotating objects of large number of particles as  $v$  is now radial and different for every particle along the radii of the object. It can be shown [6] that the moment of inertia of a rotating object about an axis of radius  $r$  is given by

$$J = \sum m_i r_i^2 = \int r^2 dm$$

where  $m$ =mass,  $r$ =radii,  $i$ = $i$ -th particle. Some texts [6] use  $I$  instead of  $J$  in the same units. When specifying the moment of inertia of a machine's rotor, we can that it is cylindrical in shape as shown in Fig.B1

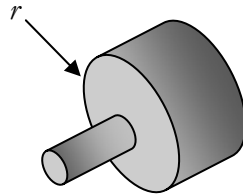


**Fig. B.1. Solid exemplifying a machine's rotor**

The moment of inertia for a rotor is then given by  $J = \frac{1}{2}mr^2$  in  $kg\cdot m^2$  where  $m$  and  $r$  are the mass and radii of the shaft respectively.

## Appendix C: Harmonic Phase-ANGLE Measurement in Simplorer®

Simplorer® provides FFT blocks that allow extracting instantaneous magnitude and phase information of any signal. The current is chosen as the HIF analysis detection criteria, so the FFT blocks act as the harmonic extraction agent. The sampling frequency can be specified to be anything, but to model realistic equipment it was set at  $f_s=10$ -kHz. The phase output of the FFT block is extracted through the PHIDEG[n] parameter, where  $n$ =harmonic order and the output is in the complete form of  $(n\omega t + \varphi_n)$ . A plot for the fundamental ( $n=1$ ) and third ( $n=3$ ) instantaneous harmonic phase-angle as presented by Simplorer® is shown in Fig.C.1.

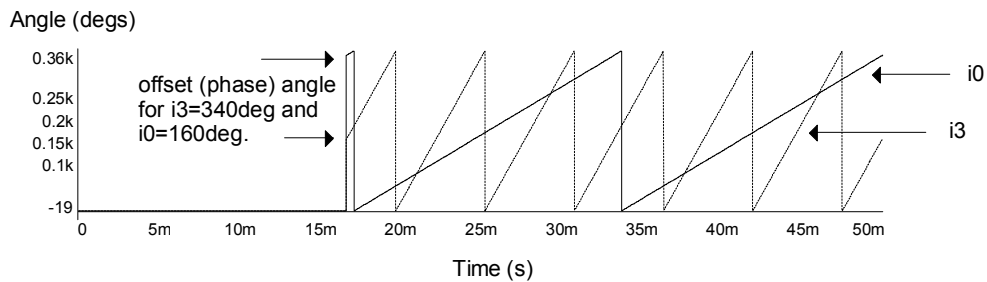


**Fig. C.1. Instantaneous harmonic phase-angle information**

The complete phase  $(n\omega t + \varphi_n)$  rises linearly from 0 to  $360^\circ$  periodically because it includes  $\omega t$ , the  $n$ -th rotating phasor, and the phase angle which is the offset in degrees. The FFT blocks take one cycle (16.67-ms) to compute the harmonic information, after which it gives the instantaneous phase-angle displacement in the form of a y-axis offset.

It is noticed how the phase for  $i_3$  varies three times faster than  $i_0$ ; this is expected since the  $3\omega t$ -phasor goes around three times faster than the  $1\omega t$ -phasor. Should there be any instantaneous change in the phase angle due to a fault or disturbance, it will be shown in the form of a a/deceleration in Fig.C.1 in either a faster (forward angle-shift) or slower (reverse angle-shift) rise. This effect is shown in Fig.C.2.

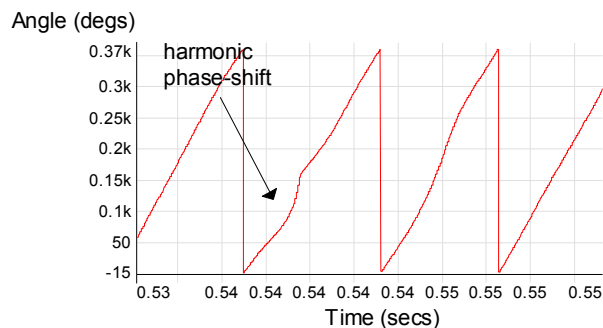


**Fig. C.2. Instantaneous harmonic phase-shift**

The angle of the harmonic shown in Fig.C.2 first shifts first backwards (decrement in slope), then forward (increment in slope). This tells us that something has disturbed the system and that the harmonic angle  $\varphi_n$  has shifted. In the case of Fig.C.2,  $\varphi_n$  returns to its original position indicating that there was only a temporary disturbance and nothing pronounced; perhaps a load dump. The change in Fig.C.2 can be compared to the phasor diagram of Fig.C.3.

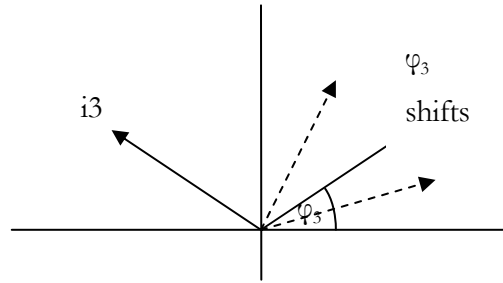


**Fig. C.3. Phasor diagram showing temporal phase-shift**

To find the angle difference between any two harmonics  $k$  and  $n$ , the following mathematical operations were applied.

$$\varphi_k - \varphi_n = [(k\omega t + \varphi_k) - k\omega t] - [(n\omega t + \varphi_n) - n\omega t]$$

were  $k\omega t$  and  $n\omega t$  were subtracted from PHIDEG[ $k$ ] and PHIDEG[ $n$ ] respectively to obtain the angle difference.

# Appendix D: Final schematic in Simplorer

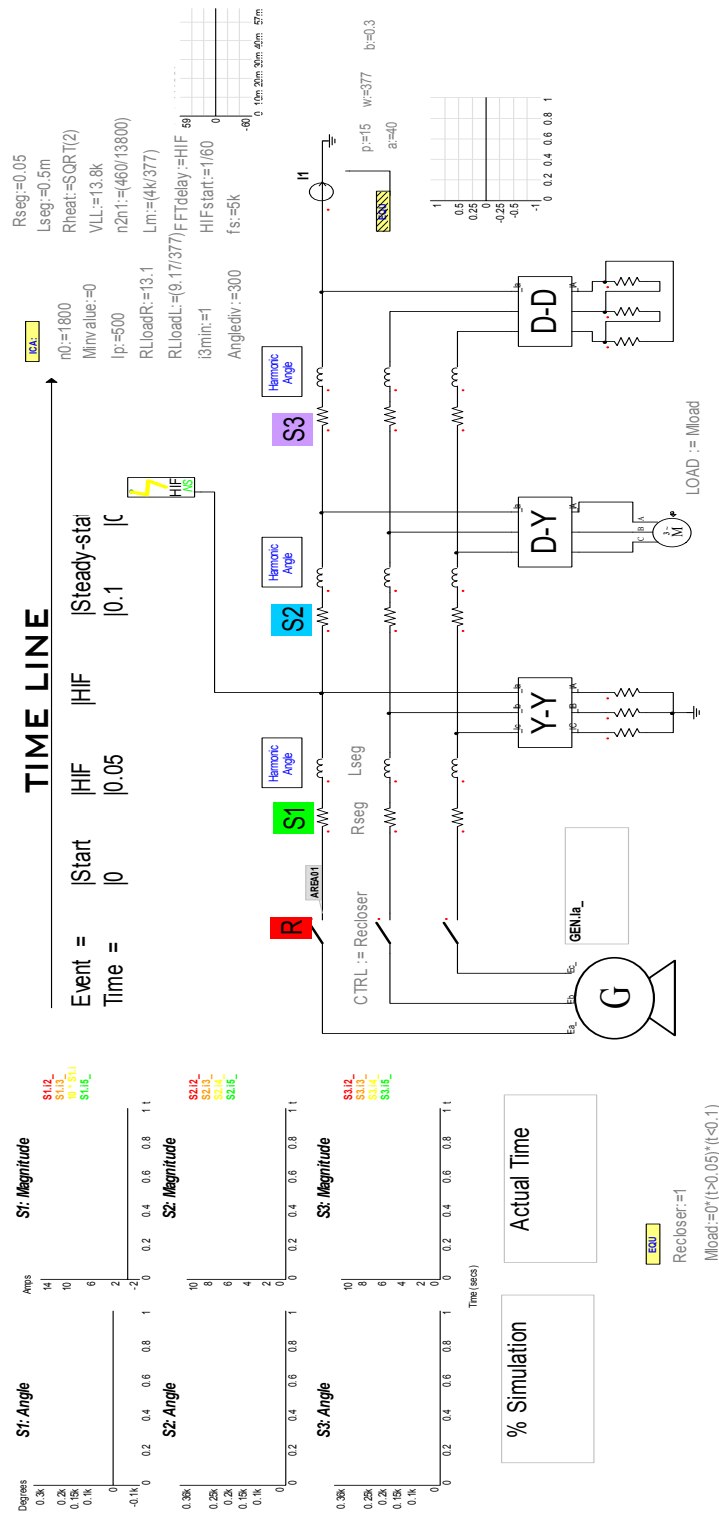


Fig. D.1. Final simulation schematic used (non-available parts in Simplorer® shown were created individually)

## REFERENCES

- [1] Hambley, Allan R. “Electrical Engineering, Principles and Applications”. Prentice Hall, 2002.
- [2] Stevenson, Jr. William D. “Elements of Power System Analysis, 4<sup>th</sup> ed.”. McGraw Hill, 1985.
- [3] Centeno, Virgilio. Lecture Notes for ECE 3354 – Power Systems and the Environment, taught during the summer of 2001.
- [4] López Aramburú, Fernando. “Circuitos Electricos II, 2da ed.” Editorial Ciencias, 2001.
- [5] Yamayee, Zia A., Bala, Jr., Juan L. “Electromechanical Energy Devices and Power Systems”. John Wiley & Sons, 1994.
- [6] Halliday, David Resnick, Robert Walker, Jearl. “Fundamentals of Physics”. John Wiley & Sons, 1997.
- [7] Krause, Paul C. “Analysis of Electric Machinery”. McGraw Hill, 1986.
- [8] Ansoft. “Simulation System SIMPLORER® 6.0 User Manual”. 2002.
- [9] Tenglin, John, et al. “High Impedance Fault Detection Technology”. Report of PSRC Working Group D15, 1996
- [10] Nam, S.R., et al. at KEPCO. “Modeling of a High Impedance Fault in a Distribution System Using Two Series Time-Varying Resistances in EMTP”. IEEE Transactions on PES.
- [11] DePablos, Juancarlo. “Internet Peer-to-Peer Communication Based Distribution Loop Control System”. Master thesis at Virginia Tech, 2003.
- [12] Jeerings, D. Linders, R. “Unique Aspects of Distribution System Harmonics Due to High Impedance Ground Faults”. IEEE Transactions on PES.
- [13] Benner, C. Russell, B. “Practical High Impedance Fault Detection on Distribution Feeders”. IEEE Transactions on PES.

- [14] Yu, David C. Khan, Shoukat H. “An Adaptive High and Low Impedance Fault Detection Method”. Prentice Hall, 2001.
- [15] Ramu, Krishnan. “Electric Motor Drives: Modeling, Analysis and Control”. Prentice Hall, 2001.
- [16] Uriarte, Fabian. “An Equation To Model Hysterisis Loops and Approximate Magnetizing Currents in Steady-State”. A currently unpublished journal.
- [17] J.M. Prousalidis, N.D. Hatziaargyriou, and B.C. Papadias. “Representation of hysterisis in three-phase transformer models for electromagnetic transients”. IEEE Transactions on PES.
- [18] U.D. Annakkage, P.G. McLaren, E.Dirks, R.P. Jayasinghe, and A.D. Parker. “A Current Transformer Model Based on the Jiles-Atherton Theory of Ferromagnetic Hysterisis”. IEEE Transactions on PES

## **VITA**

Fabian Marcel Uriarte, born on October 26, 1977 graduated with an Electrical Engineering degree from Virginia Tech in 2002. While pursuing his master's degree at Virginia Tech, he taught undergraduate level laboratories in electronics and power systems, where as a high-ranked lab instructor, he developed deeper interest in the power systems area. Various times Dean's list as an undergraduate, ranked the highest graduate-student instructor, he continues to pursue his master's researching the development of algorithms to detect high-impedance faults in distribution feeders.